Probing Higgs bosons with large bottom Yukawa coupling at hadron colliders

C. Balázs,[1,2] J. L. Diaz-Cruz,[3] H.-J. He,[1,2] T. Tait,[1,4] and C.-P. Yuan[1]
[1]*Michigan State University, East Lansing, Michigan 48824*
[2]*Fermi National Accelerator Laboratory, Batavia, Illinois 60510*
[3]*Instituto de Fisica, BUAP, 72570 Puebla, Puebla, Mexico*
[4]*Argonne National Laboratory, Argonne, Illinois 60439*
(Received 21 July 1998; published 10 February 1999)

The small mass of the bottom quark, relative to its weak isospin partner, the top quark, makes the bottom an effective probe of new physics in Higgs and top sectors. We study the Higgs boson production associated with bottom quarks, $p\bar{p}/pp \to \phi b\bar{b} \to b\bar{b}b\bar{b}$, at the Fermilab Tevatron and the CERN LHC. We find that strong and model-independent constraints on the size of the ϕ-b-$\bar{b}$ coupling can be obtained for a wide range of Higgs boson masses. Their implications for the composite Higgs models with strong dynamics associated with the third family quarks (such as the top-quark condensate or top-color models with naturally large bottom Yukawa couplings), and for the supersymmetric models with large $\tan\beta$, are analyzed. We conclude that the Tevatron and the LHC can put stringent bounds on these models, if the $\phi b\bar{b}$ signal is not found.
[S0556-2821(99)00705-5]

PACS number(s): 14.80.Cp, 12.38.Bx, 12.60.Jv, 14.65.Fy

I. INTRODUCTION

A major task for all future high energy colliders is to determine the electroweak symmetry breaking (EWSB) mechanism for generating the $(W^{\pm},Z^0)$ masses and the mechanism for the fermion mass generation [1]. Whether the two mechanisms are correlated or not is an interesting and yet to be determined issue. Given the large top quark mass ($m_t = 175.6 \pm 5.5$ GeV [2]), as high as the EWSB scale, it has been speculated that the top quark may play a special role in the EWSB. One of such ideas is that some new strong dynamics may involve a composite Higgs sector to generate the EWSB and to provide a dynamical origin for the top quark mass generation (e.g., the top-quark condensate or top-color models [3]). Another idea is realized in the supersymmetric theories in which the EWSB is driven radiatively by the large top quark Yukawa coupling [4].

In the minimal standard model (SM) there is only one Higgs doublet, which leaves a physical neutral scalar boson as the remnant of the spontaneous EWSB. The Yukawa couplings of the SM Higgs boson are determined from the relevant SM fermion masses divided by the vacuum expectation value (VEV), $v \simeq 246$ GeV. Thus, aside from the coupling to the heavy top quark, all the other SM Yukawa couplings are highly suppressed, independent of the Higgs boson mass. For the top-quark condensate or top-color type of models [3], with a composite Higgs sector, the new strong dynamics associated with the top sector plays a crucial role for generating the large top mass and (possibly) the W,Z boson masses. As to be discussed below, in this scenario, the interactions of the top-bottom sector with the composite Higgs bosons are different from that in the SM. Because of the infrared quasi-fixed-point structure [5] and the particular boundary conditions at the compositeness scale, the bottom Yukawa coupling to the relevant Higgs scalar is naturally as large as that of the top quark in such models. In the minimal supersymmetric extension of the SM (MSSM) [6], there are two Higgs doublets, whose mass spectrum includes two neutral scalars (h^0 and H^0), a pseudoscalar (A^0) and a pair of charged scalars ($H^{\pm}$). The MSSM Higgs sector contains two free parameters which are traditionally chosen as the ratio of the two Higgs VEV's ($\tan\beta = v_u/v_d$) and the pseudoscalar mass (m_A). A distinct feature of the MSSM is that in the large $\tan\beta$ region the Higgs Yukawa couplings to all the down-type fermions are enhanced by either $\tan\beta$ or $1/\cos\beta$. Among the down-type fermions, the bottom quark has the largest mass and so the largest Yukawa coupling. Thus, it represents a likely place where new physics could reveal itself experimentally. This common feature, the large bottom Yukawa coupling relative to that of the SM, present in both types of the (conceptually quite distinct) models discussed above, serves as the theoretical motivation for our analysis.

Since the third family b quark, as the weak isospin partner of the top quark, can have large Yukawa coupling with the Higgs scalar(s) in both composite and supersymmetric models, we recently proposed [7] to use the b quark as a probe of possible non-standard dynamics in Higgs and top sectors. In fact, because of the light b mass ($\simeq 5$ GeV) relative to that of the top quark ($\simeq 175$ GeV), the production of Higgs boson associated with b quarks ($p\bar{p}/pp \to \phi b\bar{b} \to b\bar{b}b\bar{b}$) may be experimentally accessible at the Fermilab Tevatron[1] or the CERN Large Hadron Collider (LHC),[2] even though the large top mass could render associated Higgs boson production with top quarks ($p\bar{p}/pp \to \phi t\bar{t}$) infeasible. As we will show, this makes it possible for the run II of the Tevatron and the LHC to confirm the various models in which the b-quark Yukawa coupling is naturally enhanced relative to the SM prediction. However, if the $\phi b\bar{b}$ signal is not found, the Tevatron and the LHC can put stringent constraints on the

[1]A $p\bar{p}$ collider with $\sqrt{s} = 2$ TeV.
[2]A pp collider with $\sqrt{s} = 14$ TeV.

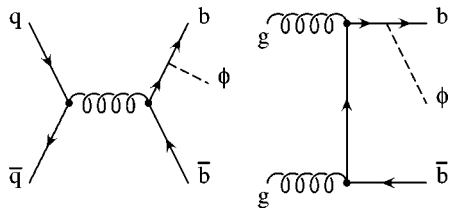

FIG. 1. Representative leading order Feynman diagrams for $\phi b\bar{b}$ production at a hadron collider. The decay $\phi \to b\bar{b}$ is not shown.

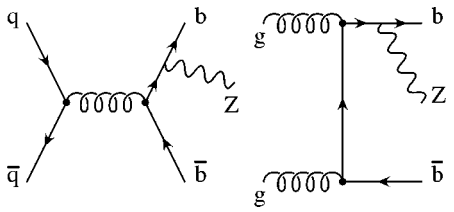

FIG. 2. Representative Feynman diagrams for leading order $Zb\bar{b}$ production at a hadron collider. The decay $Z \to b\bar{b}$ is not shown.

models with either a composite or a supersymmetric Higgs sector, in which the Yukawa coupling of the Higgs boson(s) and bottom quark is expected to be large. In Ref. [8], this reaction was explored at the LHC and the Tevatron[3] to probe the supersymmetry (SUSY) parameters of the MSSM. The conclusion was that, with efficient b tagging, useful information concerning the MSSM could be extracted from either the LHC or a high luminosity Tevatron. In this work, we expand upon earlier results [7] in which it was concluded that even the much lower integrated luminosity of the Tevatron run II can provide useful information through this reaction, provided an optimized search strategy is employed. We begin with a model-independent analysis in Sec. II, considering relevant backgrounds and determining an effective search strategy to extract a signal from the backgrounds. We then apply these results to constrain both composite and supersymmetric models in Secs. III and IV. In Sec. III, we first analyze the constraints on the two Higgs doublet extension of top-quark condensate model [9] and the top-color model [10], and then remark upon the recent dynamical left-right model [11] (as a natural extension of the minimal top-quark condensate model [12]) which also generically predict a large bottom Yukawa coupling. In Sec. IV, after deriving the exclusion contours on the m_A-tanβ plane of the MSSM, we further analyze its implication on the supergravity [13] and gauge-mediated [14] models of soft SUSY breaking that naturally predict a large tanβ. The comparison of our Tevatron run II results with the CERN e^+e^- collider LEP II bounds (from the Zh and hA channels) is also presented, illustrating the complementarity of our analysis to other existing Higgs search strategies. Final conclusions are given in Sec. V.

II. SIGNAL AND BACKGROUND

We are interested in studying production of $\phi b\bar{b} \to b\bar{b}b\bar{b}$ at the run II of the Tevatron and the LHC. The signal events result from QCD production of a primary $b\bar{b}$ pair, with a Higgs boson (ϕ) radiated from one of the bottom quark lines (cf. Fig. 1). The Higgs boson then decays into a secondary $b\bar{b}$ pair to form a $b\bar{b}b\bar{b}$ final state. Because our detection strategy relies upon observing the primary b quarks in the final state (and thus demands that they have large transverse momentum), our calculation of the $\phi b\bar{b}$ signal rate from diagrams such as those shown in Fig. 1 is expected to be reliable. This is in contrast to the *inclusive* rate of ϕ production at a hadron collider, in which one does not require a final state topology with four distinct jets. In this case a calculation based upon Feynman diagrams such as those shown in Fig. 1 may not be reliable. It would be better to consider the Higgs boson production via bottom quark fusion, such as $b\bar{b} \to \phi$ and $gb \to \phi b$, with cares to avoid double counting its production rate [15]. (This calculation would resum some large logarithms which are included in the definition of the bottom parton distribution function within the proton.) We have chosen to search in the four jet final topology because the QCD background for 3 jets is much larger than that for 4 jets, and thus it would be more difficult to extract a 3 jet signal. Since the signal consists of four b (including $\bar{b}$) jets, the dominant backgrounds at a hadron collider come from production of $Zb\bar{b} \to b\bar{b}b\bar{b}$ (cf. Fig. 2), purely QCD production of $b\bar{b}b\bar{b}$ (cf. Fig. 3) [16] and $b\bar{b}jj$, where j indicates a light quark or a gluon (c.f. Fig. 4) which can occasionally produce a b-jet like signature in the detector.

In order to derive model-independent bounds on the couplings of the scalar particles with the bottom quark, we consider K, the square-root of the enhancement factor for the production of $\phi b\bar{b} \to b\bar{b}b\bar{b}$ over the SM prediction. By definition,

$$K = \frac{y_b}{(y_b)_{\rm SM}}, \tag{1}$$

in which $(y_b)_{\rm SM} = \sqrt{2} m_b / v$ is the SM bottom Yukawa coupling and y_b is the bottom Yukawa coupling in the new physics model under the consideration.[4] The decay branching ratio of ϕ to $b\bar{b}$ is model-dependent, and is not included in the calculations of this section. [Namely, the decay branching ratio Br($\phi \to b\bar{b}$) is set to be one]. We will prop-

[3]In [8], a 1.8 TeV $p\bar{p}$ Tevatron was assumed with an integrated luminosity of 30 fb^{-1}, and the squark mixings of the MSSM were neglected.

[4]For simplicity, we ignore running effects in $(y_b)_{\rm SM}$ in this section, treating the bottom quark mass as 5 GeV at all scales. We will comment on the running effects of the Yukawa coupling in the context of specific models of new physics in Secs. III and IV.

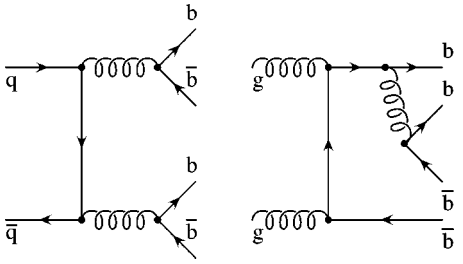

FIG. 3. Representative leading order Feynman diagrams for QCD $b\bar{b}b\bar{b}$ production at a hadron collider.

erly take it into account for the specific models to be discussed in the following sections.

We compute the signal and the backgrounds at the parton level, using leading order (LO) results from the MADGRAPH package [17] for the signal and the backgrounds, including the sub-processes initiated by $q\bar{q}$ and gg (and in the case of $b\bar{b}jj$, qg and $\bar{q}g$). While the complete next-to-leading order (NLO) calculations are not currently available for the signal or background cross sections, we draw upon existing results for high $p_T b\bar{b}$ production at hadron colliders [18] and thus estimate the NLO effects by including a k-factor of 2 for all of the signal and background rates. (NLO effects to the $pp \to \phi t\bar{t}$ cross section in the limit $s \gg m_t^2 \gg m_\phi^2$ were explored in [19]. It was found that QCD k-factor is on the order of 1.5, but this limit is not expected to provide a very good estimate to the $\phi b\bar{b}$ rate at the Tevatron since the corresponding condition $m_b^2 \gg m_\phi^2$ no longer holds. Furthermore, because the mass of the bottom quark is much less than that of the top quark, we expect that the k-factor for the $\phi b\bar{b}$ production rate to be larger than that for the $\phi t\bar{t}$ rate.) In the end of this section, we will also estimate the uncertainty in the calculation of the signal and background cross sections based upon the above prescription. We use the CTEQ4L [20] parton distribution functions (PDFs) and set the factorization scale, μ_0, to the average of the transverse masses of the primary b quarks, and the boson (ϕ or Z) transverse mass[5] for the $\phi b\bar{b}$ and $Zb\bar{b}$ processes, and use a factorization scale of $\mu_0 = \sqrt{\hat{s}}$, where $\hat{s}$ is the square of the partonic center of mass energy, for the $b\bar{b}b\bar{b}$ and $b\bar{b}jj$ background processes. It is expected that a large part of the total QCD $b\bar{b}b\bar{b}$ and $b\bar{b}jj$ rates at the Tevatron or LHC energies will come from fragmentation effects, which we have neglected in our matrix element calculation. However, due to the strong p_T and isolation cuts which we will impose for improving the signal-to-background ratio (explained below), we expect that these effects will be suppressed, and thus will only have a small effect on our results. Similarly, we expect that after imposing the necessary kinematic cuts, the signal and the background rates are less sensitive to the above choice of the factorization scale. In this section, unless otherwise noted, we will restrict our discussion of numerical results to a signal rate

[5]The transverse mass of particle i is given by $m_T^{(i)} \equiv \sqrt{m_i^2 + p_T^{(i)2}}$.

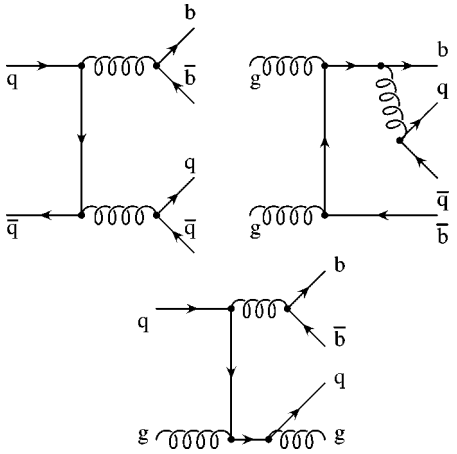

FIG. 4. Representative leading order Feynman diagrams for QCD $b\bar{b}jj$ production at a hadron collider.

corresponding to a scalar mass of $m_\phi = 100\,\mathrm{GeV}$, and an enhancement factor of $K = m_t/m_b \approx 40$. We will consider the experimental limits which may be placed on K as a function m_ϕ below.

In order to simulate the detector acceptance, we require the p_T of all four of the final state jets to be $p_T \geq 15\,\mathrm{GeV}$, and that they lie in the central region of the detector, with rapidity $|\eta| \leq 2$. We also demand that the jets are resolvable as separate objects, requiring a cone separation of $\Delta R \geq 0.4$, where $\Delta R \equiv \sqrt{\Delta\varphi^2 + \Delta\eta^2}$. ($\Delta\varphi$ is the separation in the azimuthal angles.) In the second column of Table I we present the number of events in the signal and background processes at the Tevatron run II which satisfy these acceptance cuts, assuming 2 fb^{-1} of integrated luminosity. As can be seen, the large background makes it difficult to observe a signal in the absence of a carefully tuned search strategy to enhance the signal-to-background ratio. In presenting these numbers, we have assumed that it will be possible to trigger on events containing high p_T jets (and thus retain all of the signal and background events). This capability is essential for our analysis.

The typical topology of the bottom quarks in the signal events is a ''lop-sided'' structure in which one of the bottom quarks from the Higgs boson decay has a rather high p_T of about $m_\phi/2$, whereas the other three are typically much softer. Thus, the signal events typically have one bottom

TABLE I. The signal and background events for 2 fb^{-1} of Tevatron data, assuming $m_\phi = 100\,\mathrm{GeV}$, $2\Delta m_\phi = 26\,\mathrm{GeV}$, and $K = 40$ after imposing the acceptance cuts, p_T cuts, and reconstructed m_ϕ cuts described in the text. (A k-factor of 2 is included in both the signal and the background rates.)

Process	Acceptance Cuts	p_T Cuts	ΔR Cut	ΔM Cut
$\phi b\bar{b}$	4923	1936	1389	1389
$Zb\bar{b}$	1432	580	357	357
$b\bar{b}b\bar{b}$	5.1×10^4	3760	1368	1284
$b\bar{b}jj$	1.2×10^7	1.5×10^6	6.3×10^5	5.9×10^5

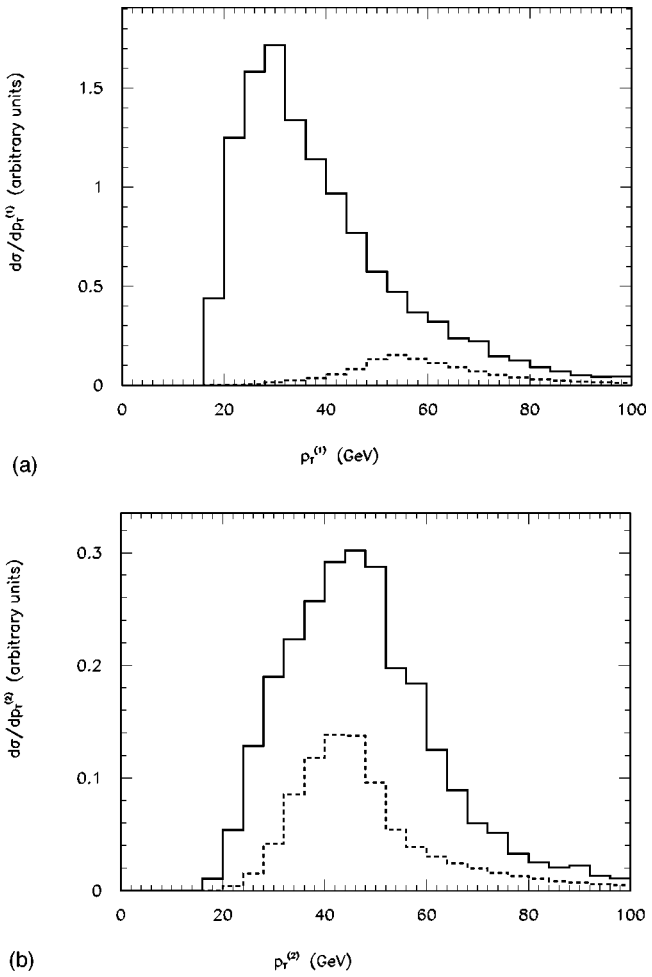

FIG. 5. Figure (a) shows the distribution of the QCD $b\bar{b}b\bar{b}$ background (solid curve) and $K=40\phi b\bar{b}$ signal (dashed curve) cross sections in $p_T^{(1)}$ at the Tevatron run II after the acceptance cuts. [$K=y_b/(y_b)_{\rm SM}$, cf. Eq. (1).] Figure (b) presents the distribution of $p_T^{(2)}$ at the Tevatron run II after applying the cut to $p_T^{(1)}$, illustrating the utility of asymmetric cuts on $p_T^{(1)}$ and $p_T^{(2)}$ in extracting the $\phi b\bar{b}$ signal from the QCD background.

quark which is much more energetic than the other three. On the other hand, the QCD $b\bar{b}b\bar{b}$ (or $b\bar{b}jj$) background is typically much more symmetrical, with pairs of bottom quarks (or fake b's) with comparable p_T. In order to exploit this, we order the b quarks by their transverse momentum,

$$p_T^{(1)}\geqslant p_T^{(2)}\geqslant p_T^{(3)}\geqslant p_T^{(4)}, \tag{2}$$

and require that the bottom quark with highest transverse momentum have $p_T^{(1)}\geqslant 50\,\text{GeV}$, and that $p_T^{(2)}\geqslant 30\,\text{GeV}$ and $p_T^{(3,4)}\geqslant 20\,\text{GeV}$.[6] In Fig. 5, we show the differential cross sections with respect to $p_T^{(1)}$ after the acceptance cuts and with respect to $p_T^{(2)}$ after the $p_T^{(1)}$ cut for the signal and the QCD $b\bar{b}b\bar{b}$ background at the Tevatron run II. These plots illustrate the advantage in isolating the signal from the background provided by the asymmetric cuts on the final state b quarks outlined above. In the third column of Table I we show the effect of these cuts on the signal and backgrounds. As can be seen, these cuts reduce the signal by about 60%, while drastically reducing the QCD $b\bar{b}b\bar{b}$ background by about 90%.

TABLE II. The optimal $p_T^{(1)}$ and $p_T^{(2)}$ cuts for isolating a Higgs boson of mass m_ϕ from the QCD $b\bar{b}b\bar{b}$ background.

m_ϕ (GeV)	$p_T^{(1)}$ Cut	$p_T^{(2)}$ Cut
75	35	25
100	50	30
125	60	35
150	70	45
175	85	55
200	90	60
250	125	80
300	150	105
350	175	190
400	190	120
500	245	160
800	390	260
1000	500	320

Since the p_T spectrum of the leading jets is determined by the mass of the scalar boson produced, the leading p_T cuts can be optimized to search for a particular m_ϕ. The results for several values of m_ϕ are presented in Table II. As expected from the discussion above, the optimal cut on $p_T^{(1)}$ is close to $m_\phi/2$ whereas the optimal cut on $p_T^{(2)}$ is somewhat lower (generally closer to $m_\phi/3$). We adopt these optimized p_T cuts for each mass considered, when estimating the search reach of the Tevatron or LHC.

Another effective method for reducing the QCD background is to tighten the isolation cut on the bottom quarks. In the QCD $b\bar{b}b\bar{b}$ background, one of the $b\bar{b}$ pairs is preferentially produced from gluon splitting. Because of the collinear enhancement, the invariant mass of this $b\bar{b}$ pair tends to be small, and the ΔR separation of these two b's prefers to be as small as possible. On the contrary, in the signal events, the invariant mass of the $b\bar{b}$ pair from the ϕ-decay is on the order of m_ϕ, and the ΔR separation is large because the angular distribution of b in the rest frame of the scalar ϕ is flat. Thus, by increasing the cut on ΔR to $\Delta R\geqslant 0.9$ we can improve the significance of the signal. As shown in column four of Table I, this cut further decreases the signal by about 30%, and the QCD $b\bar{b}b\bar{b}$ background by about 65%. In the end, their event rates are about the same.

One can further improve the significance of the signal by attempting to reconstruct the mass of the scalar resonance. This can be difficult in principle, because one does not know *a priori* what this mass is, or which bottom quarks resulted from the ϕ decay in a given event. It may be possible to

[6]Here, we have corrected the values given in Ref. [7] due to a Fortran error in evaluating the signal distribution. We thank S. Mrenna for cooperation in checking the Monte Carlo simulation and for his help in detecting this numerical error.

locate the peak in the invariant mass distribution of the secondary b quarks resulting from the ϕ decay, though with limited statistics and a poor mass resolution this may prove impractical. However, one can also scan through a set of masses, and provide 95% C.L. limits on the presence of a Higgs boson (with a given enhancement to the cross section, K) in the $b\bar{b}b\bar{b}$ data sample for each value of m_ϕ in the set. In order to do this, we assume a Higgs boson mass, and find the pair of b quarks with invariant mass which best reconstructs this assumed mass. We reject the event if this ''best reconstructed'' mass is more than $2\Delta m_\phi$ away from our assumed mass, where $2\Delta m_\phi$ is the maximum of either twice the natural width of the scalar under study (Γ_ϕ) or the twice experimental mass resolution.[7] As shown in the fifth column of Table I, this cut has virtually no effect on the signal or $Zb\bar{b}$ background (for a 100 GeV Higgs boson) while removing about another 10% of the $b\bar{b}b\bar{b}$ background.

As will be discussed below, the natural width of the Higgs bosons in both the MSSM and the models of strong EWSB that we wish to probe in this paper are generally much smaller than our estimated experimental mass resolution, and thus one might think that an improved experimental mass resolution could considerably improve the limits one may place on a scalar particle with a strong b interaction. However, the models in which we are interested generally have one or more nearly mass-degenerate bosons with similarly enhanced bottom Yukawa couplings. If the extra scalars are much closer in mass than the experimental mass resolution (and the natural width of the bosons), the signal can thus include separate signals from more than one of them. Thus there is potentially a trade-off in the ΔM cut (cf. Table I) between reduction of the background and acceptance of the signal from more than one scalar resonance. In order to estimate the potential improvement for discovering a single Higgs boson, we have examined the effect on the significance one obtains if the cut on the invariant mass which best reconstructs m_ϕ is reduced to Δm_ϕ as opposed to $2\Delta m_\phi$ as was considered above. We find that this improved mass resolution further reduces the QCD $b\bar{b}b\bar{b}$ background by about another 40%. Assuming four b tags (as discussed below), this improved mass resolution increases the significance of the signal from about 12.2 to 14.6, which will improve the model-independent lower bound on K by about 10%. Thus, an improved mass resolution would most likely be helpful in this analysis.

Another method to further suppress background rate is to observe that in the background events, the b quarks whose invariant mass best reconstructs m_ϕ come from the same gluon. This is because, after imposing all the kinematical cuts discussed above (cf. Table I), the matrix elements are dominated by Feynman diagrams in which one very far off-shell gluon decays into a $b\bar{b}$ pair, as opposed to interference of many production diagrams, which dominates the lower invariant mass region. Thus, for m_ϕ greater than about 100 GeV, the background event produces b quarks with the characteristic angular distribution of a vector decaying into fermions, $1+\cos^2\theta$, in the rest frame of the $b\bar{b}$ system. This is distinct from the signal distribution, which comes from a scalar decay, and is flat in $\cos\theta$. Thus, for masses above 100 GeV, we further require $|\cos\theta| \leq 0.7$ after boosting back to the rest frame of the $b\bar{b}$ pair which we have identified as coming from the scalar boson ϕ.

TABLE III. The signal and background events for 2 fb^{-1} of Tevatron data, assuming $m_\phi = 100$ GeV, $2\Delta m_\phi = 26$ GeV, and $K = 40$ for two or more, three or more, or four b-tags, and the resulting significance of the signal.

Process	2 or more b-tags	3 or more b-tags	4 b-tags
$\phi b\bar{b}$	1139	660	180
$Zb\bar{b}$	293	170	46
$b\bar{b}b\bar{b}$	1054	610	166
$b\bar{b}jj$	1.2×10^5	2141	4
Significance	3.3	12.21	12.25

In order to deal with the large QCD $b\bar{b}jj$ background, it is important to be able to distinguish jets initiated by b quarks from those resulting from light quarks or gluons. We estimate the probability to successfully identify a b quark passing the acceptance cuts outlined above to be 60%, with a probability of 0.5% to misidentify a jet coming from a light quark or gluon as a b jet [21]. In Table III we show the resulting number of signal and background events passing our optimized cuts at the Tevatron, assuming 2 fb^{-1} of integrated luminosity, after demanding that two or more, three or more, or four b-tags be present in the events, and the resulting significance of the signal (computed as the number of signal events divided by the square root of the number of background events). We find that requiring 3 or more b-tags results in about the same significance of 12.2σ as requiring 4 b-tags. However, we see that for the chosen parameters ($m_\phi = 100$ GeV and $K = m_t/m_b \approx 40$), even with only 2 or more b-tags, one arrives at a significance of about 3σ, and thus has some ability to probe a limited region of parameters. From the large significance, we see that the Tevatron may be used to place strong constraints on Higgs particles with enhanced bottom quark Yukawa couplings, and that the ability to tag 3 or more of the bottom quarks present in the signal can probe a larger class of models (or parameter space of the models) as compared to what is possible if only 2 or more of the bottom quarks are tagged. In the analysis below, to allow for the possibility that the $b\bar{b}jj$ background may be somewhat larger than our estimates, we require 4 b-tags, though as we have demonstrated above, we do not expect a large change in the results if 3 or 4 b-tags were required instead.

This analysis can be repeated for any value of m_ϕ, using the corresponding p_T cuts shown in Table II. It is interesting to note that the signal composition in terms of the gg or $q\bar{q}$

[7] We estimate the experimental mass resolution for an object of mass m_ϕ to be $\Delta m_\phi = 0.13 m_\phi \sqrt{100\ \text{GeV}/m_\phi}$. Under this assumption, the natural width of the bosons in the specific models of new physics considered in Secs. III and IV is usually smaller than this experimental mass resolution.

TABLE IV. Event numbers of signal (N_S), for one Higgs boson, and background (N_B) for a 2 fb^{-1} of Tevatron data and a 100 fb^{-1} of LHC data, for various values of m_ϕ, after applying the cuts described in the text, and requiring 4 b-tags. An enhancement of $K=40$ is assumed for the signal, though the numbers may be simply scaled for any $K_{\rm new}$ by multiplying by $(K_{\rm new}/40)^2$.

	Tevatron		LHC	
m_ϕ (GeV)	N_S	N_B	N_S	N_B
75	583	640	3.4×10^6	4.8×10^6
100	180	216	2.0×10^6	3.0×10^6
150	58	92	9.2×10^5	1.2×10^6
200	17	31	4.2×10^5	5.6×10^5
250	4.8	8.8	1.9×10^5	2.0×10^5
300	1.3	2.1	83000	70000
500			12000	5700
800			1500	406
1000			407	70

initial state depends on the collider type and the mass of the produced boson, which controls the type of PDF and the typical region of $x\sim m_\phi^2/S$ at which it is evaluated. At the Tevatron, for $m_\phi=100$ GeV, the signal is 99% gg initial state before cuts, and 87% after cuts, while for $m_\phi=200$ GeV, it is 99% gg initial state before cuts, and 85% after cuts. Thus, at the Tevatron, one ignores about 15% of the signal if one relies on a calculation employing only the gg initial state. At the LHC, for $m_\phi=100$, the signal is very close to 100% gg initial state before cuts and 99% after cuts, and for $m_\phi=500$ GeV, it is 99% gg initial state before cuts, and 99% after cuts. This indicates that at the LHC, very accurate results are possible from a calculation considering only the gg initial state. The resulting numbers of signal and (total) background events after cuts for various boson masses are shown in Table IV.

From these results, one may derive the minimum value of K, $K_{\rm min}$, for a scalar boson with mass m_ϕ to be discovered at the Tevatron or the LHC via the production mode $b\bar{b}\phi(\to b\bar{b})$. Similarly, if signal is not found, one can exclude models which predict the enhancement factor K to be larger than $K_{\rm min}$. To give a model-independent result, we assume that the width of the ϕ is much less than the estimated experimental mass resolution defined above, which is the case for the models studied in this paper. We determine $K_{\rm min}$ by noting that in the presence of a Higgs boson with enhanced bottom Yukawa couplings, the number of expected signal events passing our selection criterion is given by $N_S=K^2N_S^{(SM)}$, where $N_S^{(SM)}$ is the number of signal events expected for a scalar of mass m_ϕ with SM coupling to the b quark [assuming Br$(\phi\to b\bar{b})=1$], whereas the number of background events expected to pass our cuts, N_B, is independent of K. Thus, requiring that no 95% C.L. deviation is observed in the $b\bar{b}b\bar{b}$ data sample (and assuming Gaussian statistics) determines

$$K_{\rm min}=\sqrt{\frac{1.96\sqrt{N_B}}{N_S^{(SM)}}}, \tag{3}$$

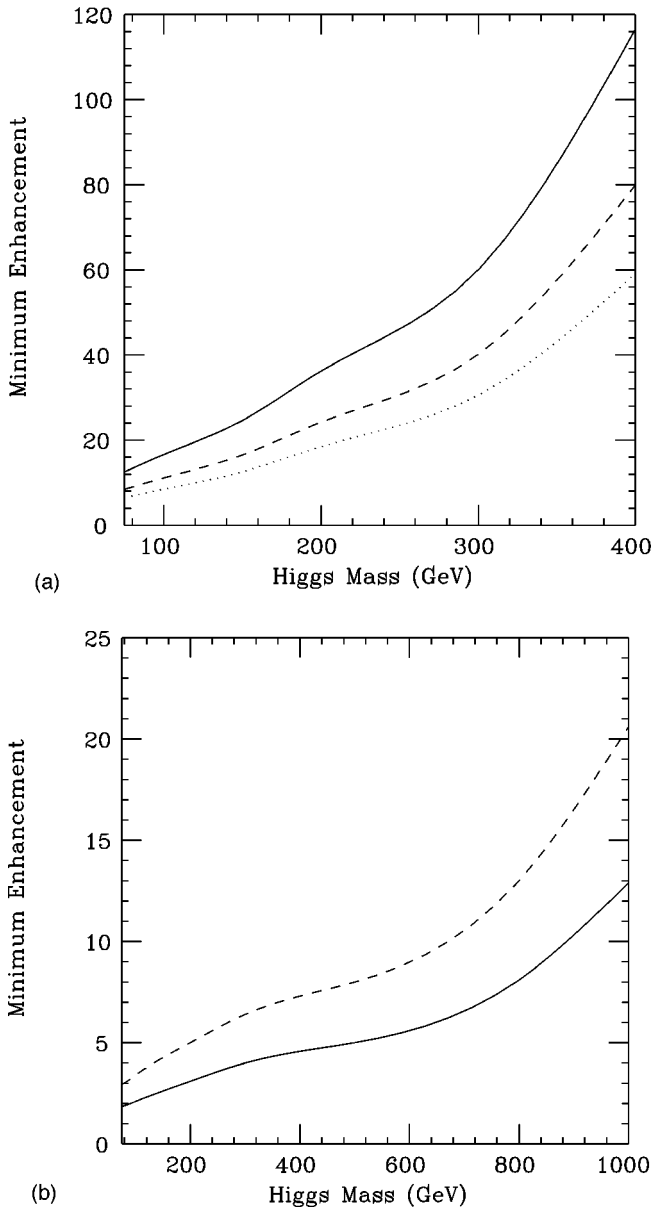

FIG. 6. (a). The model-independent minimum enhancement factor, $K_{\rm min}$, excluded at 95% C.L. as a function of scalar mass (m_ϕ) for the Tevatron run II with 2 fb^{-1} (solid curve), 10 fb^{-1} (dashed curve) and 30 fb^{-1} (dotted curve). (b). The same factor, $K_{\rm min}$, excluded at 95% C.L. (solid curve) and discovered at 5σ (dashed curve) as a function of m_ϕ for the LHC with 100 fb^{-1}. In the above, the natural width of the scalar (Γ_ϕ) is assumed to be much smaller than the experimental mass resolution.

where 1.96σ is the 95% C.L. in Gaussian statistics. In Fig. 6, we show the resulting 95% C.L. limits one may impose on $K_{\rm min}$ as a function of m_ϕ from the Tevatron with 2, 10, and 30 fb^{-1} and from the LHC with 100 fb^{-1}, as well as the discovery reach of the LHC at the 5σ level. Our conclusions concerning the LHC's ability to probe a Higgs boson with an enhanced b Yukawa coupling are very similar to those drawn in [8], but are considerably more optimistic than those in [22], where the conclusion was that the $b\bar{b}jj$ background is considerably larger than our estimate (though there are ele-

ments of the search strategy which differ between those of [22] and ours as well, and their simulation of the ATLAS detector is certainly more sophisticated). In [22] the backgrounds were simulated using PYTHIA [23] to generate two to two hard scatterings and then generating the additional jets from a parton showering algorithm. As noted above, in the light of the strong (ordering of) p_T and isolation cuts applied to select the signal events, we feel that a genuine four body matrix element calculation such as was used in our analysis provides a more reliable estimate of this background.

We have examined the scale and PDF dependence of our calculation for the signal and background rates at the Tevatron, and find that in varying the scale between one half and twice its default choice (defined above), $\mu=\mu_0/2$ and $\mu=2\mu_0$, the $\phi b\bar{b}$ signal and $Zb\bar{b}$ background rates both vary from the result at $\mu=\mu_0$ by about 30%, while the $b\bar{b}b\bar{b}$ and $b\bar{b}jj$ backgrounds vary by about 45%. This strong scale dependence is indicative of the possibility of large higher order corrections to the leading order rate. Thus, in order to better understand the true signal and background rates, it would be useful to pursue these calculations to next leading order (NLO). We have also compared the difference in the results from the Martin-Roberts-Ryskin-Stirling set R1 [MRRS(R1)] PDF [24] and the CTEQ4L PDF, and find a variation of about 10% in the resulting signal and background rates. Since these separate sources of uncertainty (from PDF and scale dependence) are non-Gaussianly distributed, there is no way to rigorously combine them. Thus, we conservatively choose to add them linearly, finding a total uncertainty of about 40% in the signal rate ($N_S^{(SM)}$), and 50% in the background rate (N_B). From the derivation of $K_{\min}$ above, we see that these uncertainties in signal and background rate (which we assume to be uncorrelated) combine to give a fractional uncertainty in $K_{\min}$,

$$\frac{\delta K_{\min}}{K_{\min}}=\sqrt{\left(\frac{\delta N_S^{(SM)}}{2N_S^{(SM)}}\right)^2+\left(\frac{\delta N_B}{4N_B}\right)^2}, \tag{4}$$

where $\delta N_S^{(SM)}$ and δN_B are the absolute uncertainties in $N_S^{(SM)}$ and N_B, respectively. From this result, we see that in terms of a more precise theoretical determination of $K_{\min}$, one gains much more from a better understanding of the signal rate than a better determination of the backgrounds. Applying our estimation of the uncertainty from PDF and scale dependence to Eq. (4), we find an over-all theoretical uncertainty in $K_{\min}$ of about 25%.

III. CONSTRAINTS AND IMPLICATIONS ON DYNAMICAL MODELS WITH STRONGLY COUPLED ELECTROWEAK SECTOR

The observed large top mass, of the order of the electroweak scale, singles out top quark from all the other light fermions. This makes the top-quark condensate or top-color scenario particularly attractive [3]. In this section, we analyze the strongly interacting scenario of the EWSB with a composite Higgs sector. We consider top-quark condensate or top-color type of models [9–12,25–28] in which new strong dynamics associated with the top quark sector plays a crucial role in the generation of the top quark and the W,Z boson masses. As we have emphasized, since the bottom quark is the weak isospin partner of the top quark, its interaction to the Higgs sector can be closely related to that of the top quark. In the top-quark condensate or top-color scenario to be analyzed below, the b quark Yukawa coupling (to the relevant scalar) is *naturally large*, of the same order as the top Yukawa coupling [$\sim O(1)$], due to the quasi-infrared fixed point structure [5] and the proper boundary conditions at the compositeness scale. This can give distinct experimental signatures at the Tevatron and the LHC. In the following, we shall analyze two specific models in this scenario, and derive the constraints (or discovery reach) expected at the Tevatron and the LHC based upon the model-independent results in Sec. II. Finally, we shall analyze the dynamical left-right symmetric extension [11] of the minimal top-quark condensate model [12].

A. In two Higgs doublet extension of the minimal top-quark condensate model

Since the minimal top-quark condensate model (with three families) [12] was ruled out due to predicting a too large top mass ($\sim 220-250\,\mathrm{GeV}$) to reconcile with experimental data, we consider the minimal two Higgs doublet extension (2HDE) of the top-condensate model proposed in Ref. [9], which predicts a smaller value of m_t. Though the simplest 2HDE of the top-quark condensate model may not provide enough reduction of the m_t value to match the Tevatron measurement, it is possible to incorporate some further improvements [3], e.g. including the recently proposed seesaw-type top-quark condensation [28], to achieve a realistic m_t. In the supersymmetrized version of the top-quark condensate model [29], it is possible to derive the correct top mass while keeping the similar boundary conditions and the quasi-infrared fixed point structure which ensures the large b quark (and also τ lepton) Yukawa couplings. In this subsection we analyze the simplest 2HDE of the top-quark condensate model constructed in Ref. [9], for illustration.

The starting point of the model is to consider the SM without an elementary Higgs boson, but with Nambu–Jona-Lasinio (NJL) type of four-Fermi interactions [30] generated at the cut-off scale Λ, where the new physics takes place. For the third generation quarks, the $SU(2)_L\otimes U(1)_Y$ invariant 4-Fermi couplings can be written as [9]

$$\begin{aligned}\mathcal{L}_{4F}=&G_t(\bar{\Psi}_L t_R)(\bar{t}_R\Psi_L)+G_b(\bar{\Psi}_L b_R)(\bar{b}_R\Psi_L)\\&+G_{tb}[(\bar{\Psi}_L b_R)(\bar{t}_R^c\tilde{\Psi}_L)+\mathrm{H.c.}],\end{aligned} \tag{5}$$

where the summation over color indices is implied in the round parentheses and $\tilde{\Psi}=(-b^c,t^c)^T$. Then, just below the scale Λ, two composite Higgs doublets, Φ_t and Φ_b, can be introduced via the auxiliary field method [31] with the interaction Lagrangian

$$\begin{aligned}\mathcal{L}_{SF}=&-\mu_t^2\Phi_t^\dagger\Phi_t+(\bar{\Psi}_L\Phi_t t_R+\mathrm{H.c.})-\mu_b^2\Phi_b^\dagger\Phi_b\\&+(\bar{\Psi}_L\Phi_b b_R+\mathrm{H.c.})-\mu_{tb}^2(\Phi_t^\dagger\Phi_b+\mathrm{H.c.}).\end{aligned} \tag{6}$$

To diagonalize the Φ_t and Φ_b mass terms, one needs to introduce the mixing angle α defined by $\alpha=2\mu_{tb}^2/(\mu_t^2-\mu_b^2)$. In Eqs. (5) and (6), the mixing term proportional to G_{tb} or μ_{tb} is important to break the Peccei-Quinn $U(1)$ symmetry and to generate a nonzero mass for the pseudoscalar. The low energy Lagrangian at the scale $\mu(<\Lambda)$ can be deduced from Eq. (6) via the renormalization group (RG) evolution [32] which defines the effective low energy couplings. Thus, at the scale μ,

$$\begin{aligned}\mathcal{L}_{SF}^{(r)}=&Z_{\Phi_t}^{1/2}y_t(\bar{\Psi}_L\Phi_t t_R+\text{H.c.})+Z_{\Phi_b}^{1/2}y_b(\bar{\Psi}_L\Phi_b b_R+\text{H.c.})\\&+Z_{\Phi_t}(D^\mu\Phi_t)^\dagger(D_\mu\Phi_t)+Z_{\Phi_b}(D^\mu\Phi_b)^\dagger(D_\mu\Phi_b)\\&+V(Z_{\Phi_t}^{1/2}\Phi_t,Z_{\Phi_b}^{1/2}\Phi_b),\end{aligned}\tag{7}$$

where V is the renormalized Higgs potential for Φ_t and Φ_b. As μ approaches to Λ, Eq. (7) should match with the bare Lagrangian (6) to result in the proper boundary conditions to be used in the renormalization group analysis [9]. It turns out that the compositeness of both Φ_t and Φ_b can be achieved only for the boundary condition $y_t(\Lambda)=y_b(\Lambda)\equiv y_0\gg 1$ [9,3]. Hence,

$$y_t(\mu)\approx y_b(\mu),\quad (\text{for any } \mu<\Lambda).\tag{8}$$

This is due to the fact that y_t and y_b satisfy similar RG equations except for a small difference (in the g_1^2 term) originating from the different hyper-charges of the t and b quarks [32,3]:

$$\begin{aligned}\frac{dy_t(\mu)}{d\ln\mu}=&\frac{1}{16\pi^2}\left[\left(\frac{3}{2}+N_c\right)y_t^2(\mu)+\frac{1}{2}y_b^2(\mu)\right.\\&-3\left(N_c-\frac{1}{N_c}\right)g_3^2(\mu)-\frac{9}{4}g_2^2(\mu)\\&\left.-\frac{17}{12}g_1^2(\mu)\right]y_t(\mu),\\\frac{dy_b(\mu)}{d\ln\mu}=&\frac{1}{16\pi^2}\left[\left(\frac{3}{2}+N_c\right)y_b^2(\mu)+\frac{1}{2}y_t^2(\mu)\right.\\&-3\left(N_c-\frac{1}{N_c}\right)g_3^2(\mu)-\frac{9}{4}g_2^2(\mu)\\&\left.-\frac{5}{12}g_1^2(\mu)\right]y_b(\mu),\end{aligned}\tag{9}$$

where $N_c=3$ for the QCD theory, and $\mu\geqslant m_t\sim M_{\text{Higgs}}$. Because of the infrared quasi-fixed point structure [5,32] of the two Higgs doublet model, the relation (8) holds well as long as $y_b(\Lambda),y_t(\Lambda)\geqslant 1$. This is true even for the case where y_b is chosen to be significantly lower than y_t at the compositeness scale Λ. This running behavior is shown in Fig. 7, which confirms the large value of y_b at the weak scale. We have also examined possible threshold effects due to different values of the Higgs masses and found the above conclusion unchanged.

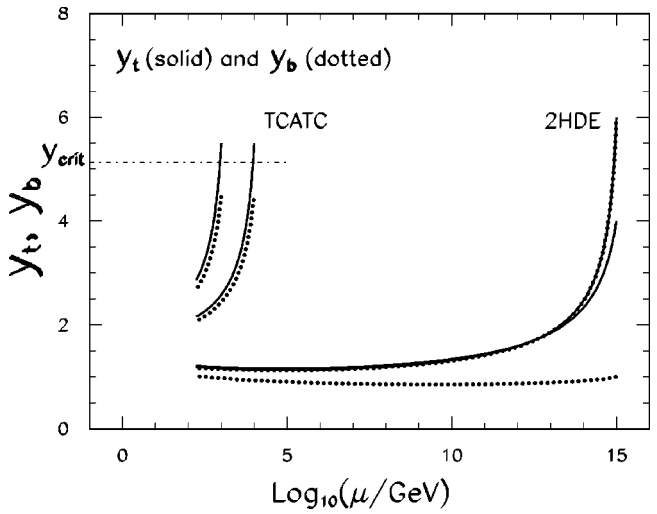

FIG. 7. Renormalization group running of y_t and y_b in the 2HDE of top-quark condensate model and the TCATC model. For the 2HDE of top-quark condensate model, two sets of curves are shown: the upper two curves (solid for y_t and dotted for y_b) are for the typical boundary condition $y_t(10^{15}\,\text{GeV})=y_b(10^{15}\,\text{GeV})=6\gg 1$ and they are too close to be distinguishable; the lower two curves are for the boundary condition $y_t(10^{15}\,\text{GeV})=4, y_b(10^{15}\,\text{GeV})=1$. In both cases, y_t and y_b have very similar infrared values, of $O(1)$, at the weak scale.

The two composite Higgs doublets develop VEVs from the condensation of $\langle\bar{t}t\rangle$ and $\langle\bar{b}b\rangle$ (determined by the gap equations), so that $\langle\Phi_t\rangle=(v_t,0)^T/\sqrt{2}$ and $\langle\Phi_b\rangle=(0,v_b)^T/\sqrt{2}$. Since the masses of the t and b quarks are given by $m_{t,b}(\mu)=y_{t,b}(\mu)v_{t,b}(\mu)/\sqrt{2}$, and the Yukawa couplings y_b and y_t are about the same, of the $O(1)$ at the weak scale [cf. Eq. (8) and Fig. 7], this model naturally *predicts* a large $\tan\beta$:

$$\tan\beta=\frac{v_t(m_t)}{v_b(m_t)}\approx\frac{m_t(m_t)}{m_b(m_t)}\approx 55\gg 1.\tag{10}$$

Here, $m_{b(t)}(m_t)$ is the running bottom (top) mass at the scale m_t. The running values of $m_b(\mu)$ and $m_t(\mu)$ are derived [33] from the measured physical pole masses $m_b^{\text{pol}}\simeq 5$ GeV [34] and $m_t^{\text{pol}}\simeq 175\,\text{GeV}$, and are dominated by the QCD evolution at scales $\lesssim O(M_{\text{Higgs}})$. At the one-loop level, the relation between the pole quark mass m_q^{pol} and the $\overline{\text{MS}}$ QCD running mass at the scale $\mu=m_q^{\text{pol}}$ is

$$m_q(m_q^{\text{pol}})=m_q^{\text{pol}}\left[1+\frac{4\alpha_s(m_q^{\text{pol}})}{3\pi}\right]^{-1}.\tag{11}$$

When running upward to any scale μ,

$$m_q(\mu)=m_q(m_q^{\text{pol}})\frac{c[\alpha_s(\mu)/\pi]}{c[\alpha_s(m_q^{\text{pol}})/\pi]},\tag{12}$$

where $c[x]=(23x/6)^{12/23}[1+1.175x]$ for $m_b^{\text{pol}}<\mu<m_t^{\text{pol}}$, and $c(x)=(7x/2)^{4/7}[1+1.398x]$ for $\mu>m_t^{\text{pol}}$ [35]. Numerically, $m_t(m_t^{\text{pol}})\simeq 166\,\text{GeV}$ and $m_b(m_t^{\text{pol}})\simeq 3$ GeV.

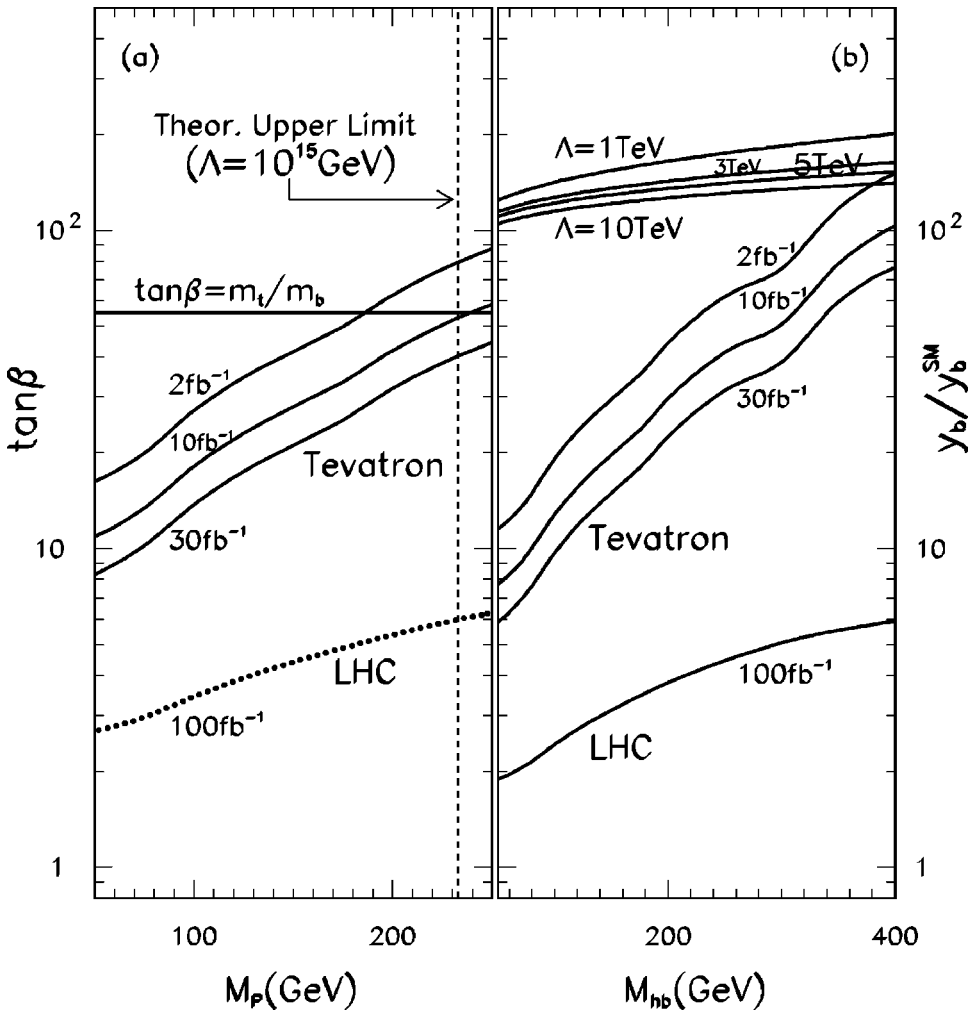

FIG. 8. 95% C.L. discovery reach of the Tevatron run II and the LHC for (a) the 2HDE of top-quark condensate model and (b) the TCATC model. Regions above the curves can be discovered. The top curves in (b) indicate $y_b(\mu = m_t)$ values for various topcolor breaking scale Λ, which are based on the RG running analysis (cf. Fig. 7).

Analyzing the mass spectrum of the Higgs sector, we find that the lightest scalar particle with the large Yukawa coupling to the bottom quark is the pseudoscalar P $(=\sqrt{2}[\sin\beta\,\mathrm{Im}\,\Phi_b^0+\cos\beta\,\mathrm{Im}\,\Phi_t^0]\sim\sqrt{2}\,\mathrm{Im}\,\Phi_b^0)$ with a mass

$$M_P \simeq \frac{v}{\sqrt{2}}|\lambda_4|^{1/2}\left[\frac{\tan(\pi-2\beta)}{\tan 2\alpha}-1\right]^{-1/2}. \qquad (13)$$

Since $v=\sqrt{v_t^2+v_b^2}\simeq 246\,\mathrm{GeV}$, M_P can be as low as $O(m_Z)$, depending on the Higgs mixing angle α and the Higgs self-couplings λ_4 [9]. For instance, for $\Lambda=10^{15}\,\mathrm{GeV}$, the mass M_P is less than about 233 GeV, and the decay branching ratio of P to $b\bar{b}$ is about one. Hence, this model predicts a light pseudoscalar that couples to the bottom quark strongly through Yukawa interaction.

To discover or exclude this model at the Tevatron and the LHC via measuring the production rate of four b jets, we need to make use of the model-independent results obtained in Sec. II. Namely, we need to compare the predicted bottom Yukawa coupling $[y_b^P=y_b(\mu)\sin\beta]$ of the pseudoscalar P with the model-independent bound $(=K_{\min}y_{b0}^{\mathrm{SM}})$ derived in Sec. II, where the reference value y_{b0}^{SM} is arbitrarily chosen to be $y_{b0}^{\mathrm{SM}}=\sqrt{2}m_b^{\mathrm{pol}}/v$ with $m_b^{\mathrm{pol}}\simeq 5$ GeV and $v\simeq 246\,\mathrm{GeV}$. This is equivalent to comparing $y_b^P/y_{b0}^{\mathrm{SM}}$ with $K_{\min}$, where y_b^P is the running Yukawa coupling at the scale M_P. Note that at the weak scale the running effects of the VEVs [mainly due to the electroweak corrections] are negligible [33], and for $\mu\lesssim M_P$, $m_b(\mu)=y_b(\mu)v_b=y_b^{\mathrm{SM}}(\mu)v$, so that $y_b^P(\mu)=\sin\beta\,y_b(\mu)=\tan\beta\sqrt{2}m_b(\mu)/v$. We can thus derive a minimal $\tan\beta$ value for a given M_P to discover such a model at hadron colliders. The result of 95% C.L. exclusion contours is given in Fig. 8 for various colliders. As shown in Fig. 8, the 2 fb^{-1} Tevatron run II data can exclude models with M_P up to $\sim 190\,\mathrm{GeV}$, if no signal is found. The entire mass range of P predicted in this model (less than 233 GeV for $\Lambda=10^{15}\,\mathrm{GeV}$) can already be explored at the Tevatron run II with a $10\,\mathrm{fb}^{-1}$ luminosity.

B. In top-color assisted technicolor model

The minimal top-quark condensate model [12] and its two-Higgs-doublet extension [9] require fine-tuning the four-Fermi coupling(s) at the scale Λ to be very close to the critical value, but do not address the dynamical origin of the effective coupling(s) at the energy scale above Λ. The top-color assisted technicolor models (TCATC) [10] were proposed to overcome such difficulties. These models postulate a gauge structure $\mathcal{G}=SU(3)_1\otimes SU(3)_2\otimes U(1)_1\otimes U(1)_2\otimes SU(2)_W$ at the scales above $\Lambda=O(1\,\mathrm{TeV})$. The third fam-

ily fermions couple to $SU(3)_1 \otimes U(1)_1$ gauge sector with the same quantum numbers as those under the SM QCD and $U(1)_Y$ interactions, while the first two family fermions couple to $SU(3)_2 \otimes U(1)_2$ in a similar way. At the scale $\Lambda = O(1\,\mathrm{TeV})$, $SU(3)_1 \otimes U(1)_1$ is strong but not confining, and $\mathcal{G}$ is spontaneously broken down to $\mathcal{G}_{\mathrm{SM}} = SU(3)_c \otimes U(1)_Y \otimes SU(2)_W$ due to an unspecified mechanism which may or may not be related to the EWSB. In consequence, massive gauge bosons of the color octet B^a (colorons) and the singlet Z' are generated. Below this breaking scale $\Lambda = \min(M_B, M_{Z'})$, 4-Fermi interactions are generated as follows:

$$\mathcal{L}_{4F} = \frac{4\pi}{\Lambda^2}\left\{\left[\kappa + \frac{2\kappa_1}{9N_c}\right](\bar{\Psi}_L t_R)(\bar{t}_R \Psi_L) + \left[\kappa - \frac{\kappa_1}{9N_c}\right](\bar{\Psi}_L b_R)(\bar{b}_R \Psi_L)\right\}. \tag{14}$$

After the fermions condense, an effective Lagrangian with two composite Higgs doublets (Φ_t and Φ_b) can be introduced as

$$\mathcal{L}_{SF} = [y_t \bar{\Psi}_L \Phi_t t_R + y_b \bar{\Psi}_L \Phi_b b_R + \mathrm{H.c.}] - \Lambda^2[\Phi_t^\dagger \Phi_t + \Phi_b^\dagger \Phi_b], \tag{15}$$

with

$$y_t = \sqrt{4\pi(\kappa + 2\kappa_1/9N_c)}, \quad y_b = \sqrt{4\pi(\kappa - \kappa_1/9N_c)}. \tag{16}$$

Here κ and κ_1 originate from the strong $SU(3)_1$ and $U(1)_1$ dynamics, respectively. The $U(1)_1$ force is attractive in the $\langle \bar{t}t \rangle$ channel but repulsive in the $\langle \bar{b}b \rangle$ channel, such that the top but not the bottom acquires dynamical mass under the condition

$$y_b < y_{\mathrm{crit}} = \sqrt{\frac{8\pi^2}{3}} < y_t. \tag{17}$$

Equivalently, this implies that the composite Higgs Φ_t but not Φ_b develops a VEV, i.e., $v_t \neq 0$ and $v_b = 0$, in contrast to the simplest 2HDE of top-quark condensate model analyzed in the previous subsection (where $v_{t,b} \neq 0$). For $\mu < \Lambda$, the composite Higgs doublets Φ_t and Φ_b develop the gauge invariant kinetic terms

$$\mathcal{L}_{SF}^{\mathrm{kin}} = Z_{\Phi_t}(D^\mu \Phi_t)^\dagger (D_\mu \Phi_t) + Z_{\Phi_b}(D^\mu \Phi_b)^\dagger (D_\mu \Phi_b),$$

$$\text{with} \quad Z_{\Phi_{t,b}} = \frac{N_c}{8\pi^2} y_{t,b}^2 \ln\frac{\Lambda}{\mu}, \tag{18}$$

as well as a potential term $V(Z_{\Phi_t}^{1/2}\Phi_t, Z_{\Phi_b}^{1/2}\Phi_b)$.

From Eq. (16), we note that unless κ_1 is unnaturally large (compared to κ), both y_t and y_b should be close to the critical value $y_{\mathrm{crit}} = \sqrt{8\pi^2/3} \simeq 5.13$ at the scale Λ. At the lower energy scale $\mu (< \Lambda)$, y_b is still close to y_t, based on the RG analysis shown in Fig. 7. From the RG evolution, we find

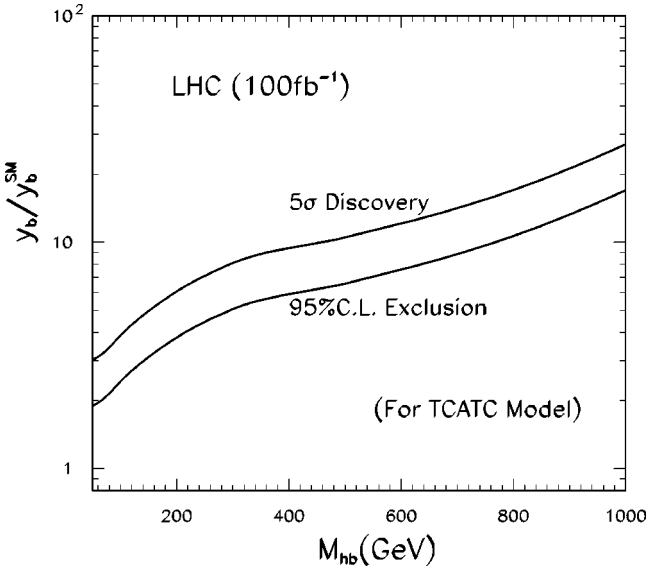

FIG. 9. The 5σ discovery and 95% C.L. exclusion contours for $y_b(\mu)/y_b^{\mathrm{SM}}(\mu)$ as a function of M_{h_b} in the TCATC model, at the LHC with 100 fb^{-1} luminosity.

$y_b(m_t) = 2.7 - 2.1$ and $y_t(m_t) = 2.9 - 2.2$ for $\Lambda = 1 - 10\,\mathrm{TeV}$, with the typical boundary conditions $y_t(\Lambda) = 5.5$ and $y_b(\Lambda) = 4.5$. The precise boundary values of $y_{t,b}(\Lambda)$ depends on the detailed dynamics of top-color breaking via the parameters (κ, κ_1). But for (κ, κ_1) not much larger than $O(1)$, $y_{b,t}(\Lambda)$ should be reasonably close to the critical value y_{crit} at the scale Λ. Furthermore, as shown in Fig. 7, the infrared behavior of $y_{t,b}(\mu)$ at the weak scale is not sensitive to the possible variations of their boundary values at the scale Λ. Therefore, this model generically predicts a large y_b of $O(2-3)$ at the weak scale.

Another essential feature of the TCATC model [10] is that the top-color interaction must not be responsible for the whole EWSB, but is mainly responsible for the top quark mass generation. As a result, the dynamical scale can be as low as $\Lambda = O(1)$ TeV (which avoids the severe fine-tuning needed in the minimal models [9,12]) and correspondingly, $v_t \simeq 64 - 97\,\mathrm{GeV}$ (for $\Lambda = 1 - 10\,\mathrm{TeV}$) according to the Pagels-Stokar formula [36]:

$$v_t^2 = \frac{N_c}{8\pi^2} m_t^2 \left(\ln\frac{\Lambda^2}{m_t^2} + c_0\right) \tag{19}$$

where $c_0 = O(1)$ is a constant. The b quark gets large portion of its mass from top-color instanton effects [10]. The EWSB is mainly driven by the usual extended technicolor (ETC) [37,38] (or the equivalent Higgs) interaction which gives small masses [$\lesssim O(\mathrm{GeV})$] to all fermions (including t and b). In addition, this model predicts three physical top-pions with masses around $O(150$–$300)$ GeV. The smaller vacuum expectation value v_t [estimated by Eq. (19) in TCATC models], as compared to the full VEV ($v \simeq 246\,\mathrm{GeV}$), makes the Yukawa coupling of the top to Φ_t stronger than that in the SM, which is consistent with the predictions from the RG analysis in Fig. 7. The large-N_c calculation [39] suggests that

the neutral components (h_b, A_b) of Φ_b are degenerate and can be the lightest Higgs bosons with masses of $O(100)$ GeV to a few hundred GeV. Hence, this model also predicts light scalars which couple to the bottom quark strongly via Yukawa interaction.

To illustrate how Tevatron (run II) and LHC can test this model via the reaction $p\bar{p}/pp \to b\bar{b}h(\to b\bar{b}) + X$, we compare $y_b(\mu)$ (predicted in Fig. 7) with the model-independent bound on $K_{\min} y_{b0}^{\rm SM}$ derived in Sec. II. Or, equivalently, we compare $y_b(\mu)/y_b^{\rm SM}(\mu)$ with $K_{\min} y_{b0}^{\rm SM}/y_b^{\rm SM}(\mu)$ $[=K_{\min} m_b^{\rm pol}/m_b(\mu)]$. The result is shown in Fig. 8b. It is clear that the Tevatron run II can already provide important information on this type of models. The LHC data can further extend the coverage of the mass range up to $O(1)$ TeV. In Fig. 9, we present the exclusion curve at the 95% C.L. and the discovery reach at the 5σ level for the LHC with 100 fb^{-1} of luminosity. If we relax the mass degeneracy condition (as suggested by the large-N_c analysis) and assume that the degeneracy of h_b and A_b does not hold well enough to be within the mass resolution of the detector (cf. Sec. II), then the contours in Figs. 8 and 9 will move up by an overall factor of $\sqrt{2}$ for most of the mass region. Figure 9 shows that even in this non-degeneracy case, the LHC (with a 100 fb^{-1} luminosity) can discover the Higgs boson h_b or A_b with a mass up to 1 TeV at the 5σ level, since the theory curves always lie above $y_b/y_b^{\rm SM}=100$ for $M_{h_b(A_b)} \geqslant 50$ GeV (cf. Fig. 8b).

C. In dynamical left-right symmetric extension of the top-quark condensate model

Finally, we consider the left-right symmetric extension [11] of the top-quark condensate model, which postulates the gauge structure $\mathcal{G}_{\rm LR}=SU(3)_c\otimes SU(2)_L\otimes SU(2)_R \otimes U(1)_{B-L}$ at a high energy scale Λ. This model has many attractive features. For example, parity violation can appear naturally via the spontaneous symmetry breaking and the known quarks and leptons fit economically into fundamental representations of the gauge group. A dynamical see-saw mechanism can also be realized in this scenario, which naturally yields the small neutrino masses.

At the compositeness scale Λ, a set of NJL-type four-Fermi interactions are generated, which produce a composite Higgs sector at the lower scale $\mu(<\Lambda)$. The symmetry breaking pattern occurs via two steps: first, $\mathcal{G}_{LR}$ breaks down to $\mathcal{G}_{\rm SM}=SU(3)_c\otimes SU(2)_L\otimes U(1)_Y$ at a scale $\mu=\Lambda_{\rm R}$; second, the remaining standard model group $\mathcal{G}_{\rm SM}$ is broken down to $SU(3)_c\otimes U(1)_{\rm em}$ at the electroweak scale of $O(100\,{\rm GeV})$. The composite Higgs sector of this model contains a scalar bi-doublet Φ, two scalar doublets χ_L and χ_R, and a singlet scalar σ, with the quantum number assignments (1,2,2,0), (1,2,1,-1), (1,1,2,-1) and (1,1,1,0), respectively. They are defined as

$$\Phi=\begin{pmatrix} \dfrac{\phi_1^0+v_1}{\sqrt{2}} & \phi_2^+ \\ \phi_1^- & \dfrac{\phi_2^0+v_2}{\sqrt{2}} \end{pmatrix}, \quad \chi_L=\begin{pmatrix} \dfrac{\chi_L^0+v_L}{\sqrt{2}} \\ \chi_L^- \end{pmatrix},$$

$$\chi_R=\begin{pmatrix} \dfrac{\chi_R^0+v_R}{\sqrt{2}} \\ \chi_R^- \end{pmatrix}, \quad \sigma, \tag{20}$$

where the vacuum expectation value v_R is much larger than the other VEVs ($v_{1,2}$ and v_L) and is responsible for the first step breaking of the left-right symmetry. The true VEV ($v \simeq 246$ GeV) for the EWSB is determined by

$$v^2=(v_1^2+v_2^2)+\frac{1}{2}[(v_R^2+v_L^2)-\sqrt{(v_R^2-v_L^2)^2+(4v_1v_2)^2}]$$
$$\simeq v_1^2+v_2^2+v_L^2, \tag{21}$$

where the approximate relation holds, because $v_R \gg v_{1,2}, v_L$. Note that a nonzero v_L (which may be relatively small) implies $v_{12}\equiv\sqrt{v_1^2+v_2^2}<v\simeq 246$ GeV. Furthermore, the singlet scalar σ does not develop VEV.

The relevant Yukawa interactions and mass terms for the top-bottom sector can be written as [11]:

$$\mathcal{L}_{SF}^{tb}=m_t\bar{t}t+m_b\bar{b}b+\frac{1}{\sqrt{2}}\bar{t}(y_1\phi_1^0+y_2\phi_2^0)t$$
$$+\frac{1}{\sqrt{2}}\bar{b}(y_1\phi_2^0+y_2\phi_1^0)b+[\bar{b_L}(y_1\phi_1^- - y_2\phi_2^-)t_R$$
$$+\bar{t}_L(y_1\phi_2^+ - y_2\phi_1^+)b_R+{\rm H.c.}],$$
$$m_t=(y_1v_1+y_2v_2)/\sqrt{2}, \quad m_b=(y_1v_2+y_2v_1)/\sqrt{2}, \tag{22}$$

which only involve the scalars in the bi-doublet Φ. To give the correct top mass, $\tan\beta$ ($\equiv v_1/v_2$) is constrained to be in the range of 1.3–4.0. The formation of dynamical condensates or the VEVs of the composite Higgs scalars requires the Yukawa couplings $y_{1,2}$ to be above their critical value at the compositeness scale. Consequently, $y_{1,2}$ at the weak scale can be naturally large [of $\sim O(1)$]. The RG analysis [11] indeed shows that for Λ to be in the range of 10^5 to 10^{19} GeV, the Yukawa coupling $y_1(\mu)$ varies from about 2.1 to 1.2 at the scale $\mu=O(100-1000)$ GeV. Since the Yukawa coupling $y_2(\mu)$ satisfies the same RG equation as that of $y_1(\mu)$ (after interchanging y_1 and y_2) [11], the infrared value of $y_2(\mu)$ is also naturally large [of $O(1)$], and is not sensitive to the boundary condition at the compositeness scale.[8] Furthermore, the mass of the neutral CP-even and CP-odd scalars Re(ϕ_2^0) and Im(ϕ_2^0) may be as light as about $O(100)$ GeV [11]. We thus expect that measuring the production rate of these light scalar bosons via the $\phi b\bar{b}$ mode at the Tevatron and the LHC can effectively test this model.

Before concluding this section, we note that in the three types of dynamical models discussed above, the relevant composite Higgs scalars (having large Yukawa coupling y_b)

[8]Here, the compositeness scale Λ can be as low as 100 TeV and the left-right breaking scale $\Lambda_{\rm R}=v_R$ is around of $O(10\,{\rm TeV})$ [11].

TABLE V. Comparison of the neutral MSSM Higgs couplings to up-type ($U=u,c,t$) and down-type ($D=d,s,b;e,\mu,\tau$) fermions and to the gauge-boson ($V=W,Z$) pairs. The ratios to the corresponding SM couplings are shown, which are determined by angles β and α at the tree level.

Higgs	A	h	H
$y_U/y_U^{\rm SM}$	$\cot\beta$	$\cos\alpha/\sin\beta$	$\sin\alpha/\sin\beta$
$y_D/y_D^{\rm SM}$	$\tan\beta$	$-\sin\alpha/\cos\beta$	$\cos\alpha/\cos\beta$
$g_{\phi VV}/y_{\phi VV}^{\rm SM}$	0	$\sin(\beta-\alpha)$	$\cos(\beta-\alpha)$

do not couple to $\tau^-\tau^+$ mode at the tree level. This is in contrast to the case of MSSM where the lepton-Higgs Yukawa couplings (such as A-τ^+-τ^- etc) are enhanced in the same way as that for the down-type quarks in the large $\tan\beta$ region. Therefore, further combining the $b\bar{b}\phi$ ($\rightarrow\tau^-\tau^+$) channel into our analysis would be useful to discriminate the above dynamical models from the MSSM,[9] should a signal be observed.

IV. CONSTRAINTS ON MSSM PARAMETERS AND IMPLICATIONS FOR MODELS OF SOFT-BREAKING OF SUSY

Supersymmetry (SUSY) is one of the most natural extensions of the SM, mainly because of its ability to solve the hierarchy problem, as well as for its capacity to imitate the current experimental success of the SM, despite the plethora of the introduced new particles and free parameters [13]. The minimal supersymmetric SM (MSSM) [6] requires a two Higgs doublet extension of the SM [1] together with the corresponding supersymmetric partners. The model includes all renormalizable interactions that respect the standard gauge group $SU(3)_C\otimes SU(2)_L\otimes U(1)_Y$ and supersymmetry. In order to prevent potentially dangerous baryon and lepton number violating interactions, invariance under a discrete R-parity[10] is also required. To be compatible with data, supersymmetry has to be broken. The breaking of SUSY is parametrized by the general set of soft-breaking terms, which, in principle, should be deduced from a specific underlying model for SUSY breaking, such as the supergravity [13] and gauge-mediated [14] models. In this section, we discuss the potential of the Tevatron and the LHC to test MSSM via measuring the production rate of $\phi b\bar{b}$ mode. We shall also discuss the implication of this result on various supergravity and gauge-mediated models of soft SUSY breaking.

A. Bottom Yukawa couplings and the MSSM Higgs sector

In the MSSM, the Higgs couplings to the SM fermions and gauge bosons involve two new free parameters at the tree level, which are the vacuum angle $\beta(\equiv\arctan v_u/v_d)$ and the Higgs mixing angle α. These couplings are shown in Table V. We see that the MSSM Higgs couplings to the gauge boson pairs are always suppressed relative to that of the SM, while their couplings to the down(up)-type fermions are enhanced in the large (small) $\tan\beta$ region. These enhanced Yukawa couplings are of great phenomenological importance for the Higgs detection and especially for probing the associated new dynamics in the top-bottom sector. Alternatively, we can choose $\tan\beta$ and the pseudoscalar mass m_A as two free parameters. Then, at the one-loop level, α can be calculated from

$$\tan 2\alpha=\tan 2\beta\,(m_A^2+m_Z^2)\left[m_A^2-m_Z^2+\frac{\epsilon_t}{\cos 2\beta}\right]^{-1}, \quad (23)$$

with $\alpha\in(-\pi/2,\,0)$. Here the parameter ϵ_t represents the dominant top and stop loop corrections which depend on the fourth power of the top mass m_t and the logarithm of the stop mass $M_{\tilde{t}}^2$:

$$\epsilon_t=\frac{3G_F m_t^4}{\sqrt{2}\pi^2\sin^2\beta}\log\left(\frac{M_{\tilde{t}}^2}{m_t^2}+1\right). \quad (24)$$

Note that for large $\tan\beta$, the bottom and sbottom loop corrections can also be important. Hence, in our numerical analysis below (cf. Sec. IV B), we have included the complete radiative corrections with full mixing in the stop and sbottom sectors, and the renormalization group improvements are also adopted.[11] As shown in Table V, the A-b-$\bar{b}$ coupling has no explicit α dependence. The bottom Yukawa couplings y_{bbh} and y_{bbH} are α- and β-dependent, their magnitudes relative to the SM prediction are displayed in Fig. 10(a) as a function of m_A for various $\tan\beta$ values. It shows that for m_A above $\sim$110 GeV, the h-b-$\bar{b}$ coupling quickly decreases, approaching to the SM value for all $\tan\beta$, while the H-b-$\bar{b}$ coupling increases for large $\tan\beta$. Therefore, we expect that in the large $\tan\beta$ region, the production rate of $Ab\bar{b}$ or $hb\bar{b}$ can be large for small m_A, while the rate of $Ab\bar{b}$ or $Hb\bar{b}$ are enhanced for large m_A. Whether the signals of the two Higgs scalars (A and h, or A and H) can be experimentally resolved as two separate signals (e.g., two bumps in the $b\bar{b}$ invariant mass distribution) depends on their mass degeneracy.

[9]The τ Yukawa couplings to other possible composite scalars are not yet well specified in the top-quark condensate or top-color models, while for the dynamical left-right model the τ Yukawa couplings are expected to be naturally small, not much different from the SM value [11,40].

[10]The R-parity is defined in such a way that SM particles are even under R and their superpartners are odd.

[11]We have used the HDECAY program [35] to compute the Higgs masses, couplings and decay branching ratios.

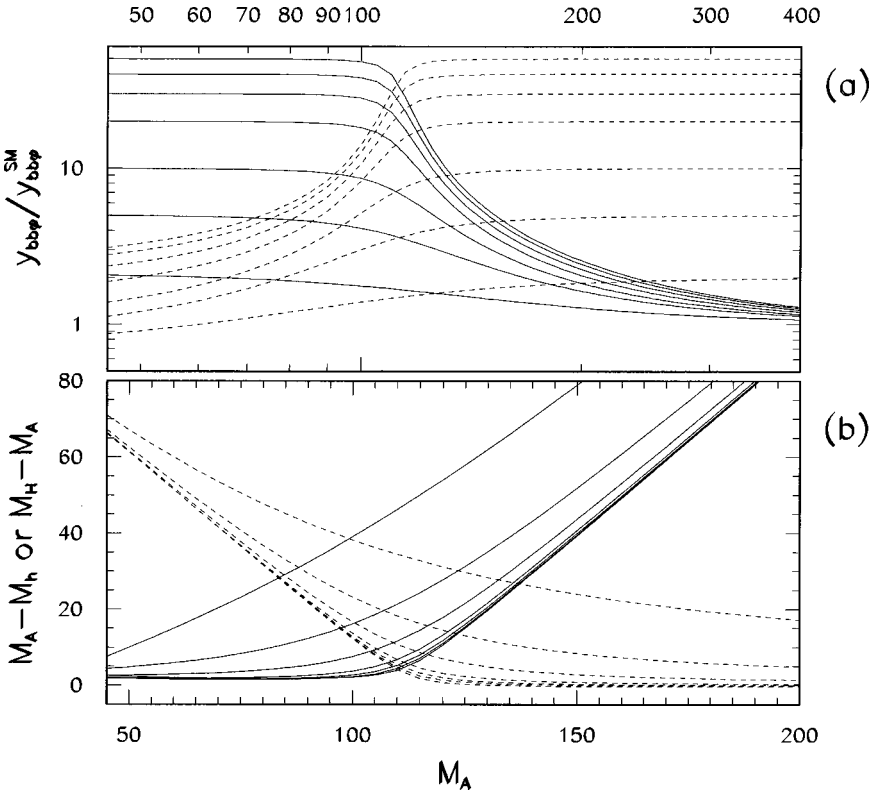

FIG. 10. Bottom Yukawa couplings to the MSSM Higgs bosons and the mass differences, $m_A - m_h$ and $m_H - m_A$, as a function of m_A for tanβ values: 2.0, 5.0, 10.0, 20.0, 30.0, 40.0, 50.0. In (a), y_{bbh} is in solid and y_{bbH} is in dashed, and tan β decreases from top to bottom curves. In (b), $m_A - m_h$ is in solid, $m_H - m_A$ is in dashed, and tanβ increases from the top to bottom curves. Here, all the SUSY soft-breaking mass parameters are chosen to be 500 GeV.

The MSSM Higgs boson mass spectrum can be determined by taking the second derivative on Higgs effective potential with respect to the Higgs fields. At tree-level, the resulting Higgs masses obey the relations: $m_h \leqslant m_Z \cos 2\beta$, $m_Z \leqslant m_H$, $m_h \leqslant m_A \leqslant m_H$, and $m_W \leqslant m_{H^\pm}$. However, these relations are substantially modified by radiative corrections [41]. Including the important contributions from top and stop loops, the masses of h and H can be written as

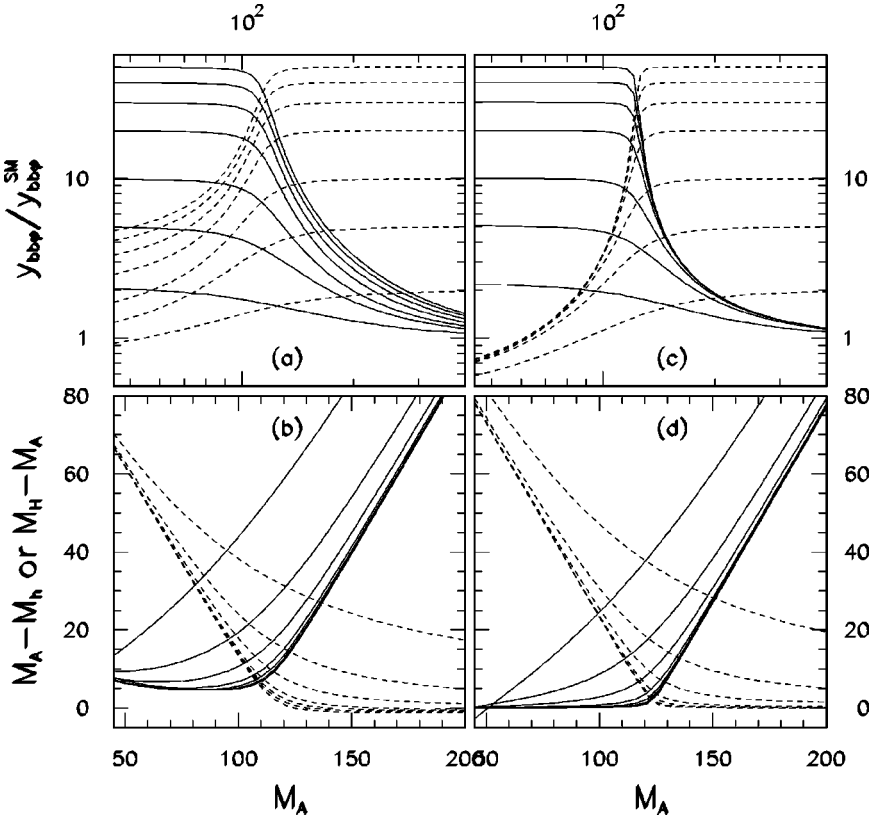

FIG. 11. The same as the previous figure, but in (a),(b), we change the right-handed stop mass to 200 GeV, and in (c),(d), we use the ''LEP II Scan A2'' set of SUSY parameters.

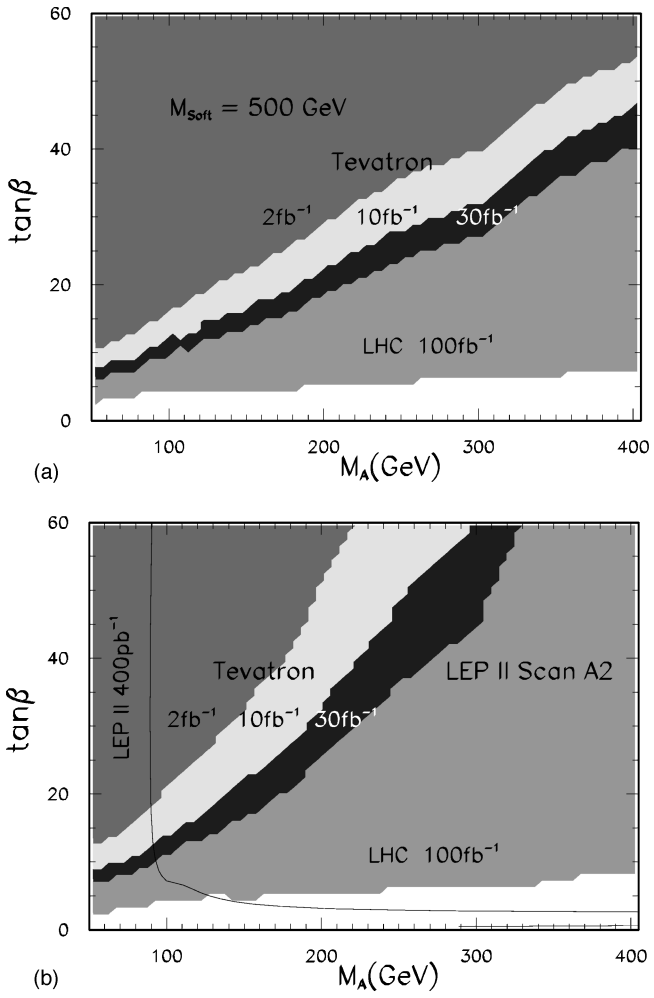

FIG. 12. 95% C.L. exclusion contours in the m_A-tanβ plane of the MSSM. The areas above the four boundaries are excluded for the Tevatron run II with the indicated luminosities, and for the LHC with an integrated luminosity of 100 fb^{-1}. The soft SUSY breaking parameters were chosen uniformly to be 500 GeV in (a), while the inputs of the ''LEP II Scan A2'' are used for the (b) in which LEP II excludes the left area of the solid curve.

$$m_{h,H}^2=\frac{1}{2}\{(M^2+\epsilon_t)\mp[(M^2+\epsilon_t)^2-4\epsilon_t(m_Z^2\cos^2\beta + m_A^2\sin^2\beta)-4m_Z^2m_A^2\cos^2 2\beta]^{1/2}\}, \quad (25)$$

where $M^2\equiv m_Z^2+m_A^2$ and the parameter ϵ_t is defined in Eq. (24). To analyze the Higgs mass degeneracies, we plot the mass differences m_A-m_h and m_H-m_A in Fig. 10(b) using the complete radiative corrections to the Higgs mass spectrum [35]. We see that for the large tanβ values, the pseudoscalar A is about degenerate in mass with the lighter neutral scalar h below $\sim$120 GeV and with the heavier neutral H above $\sim$120 GeV. This degeneracy indicates that the $\phi b\bar{b}$ signal from the MSSM generally contains two mass-degenerate scalars with similar couplings, and thus results in a stronger bound on tanβ by about a factor of $\sqrt{2}$.

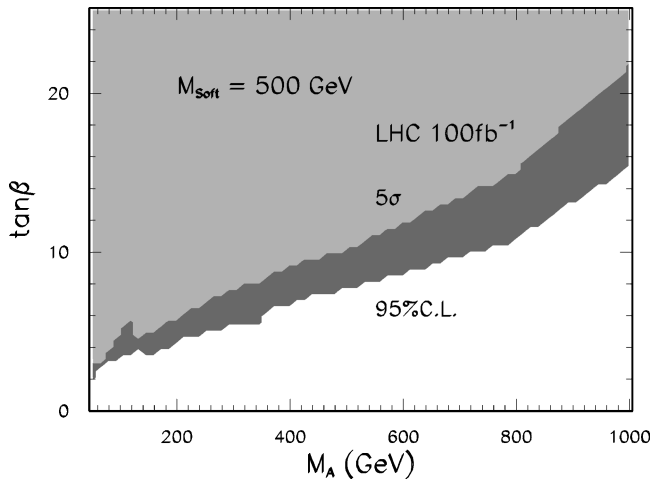

FIG. 13. Discovery and exclusion contours in the m_A-tanβ plane of the MSSM for the LHC with an integrated luminosity of 100 fb^{-1}. The area above the lower boundary is excluded at 95% C.L., while the upper boundary is the 5σ discovery contour. The soft SUSY breaking parameters were chosen uniformly to be 500 GeV.

Finally, we note that in Fig. 10, all soft-breaking mass parameters were chosen to be 500 GeV. Various choices of SUSY soft-breaking parameters typically affect these quantities by about 10–30%. To illustrate these effects, we plot in Fig. 11 the same quantities, but changing the right-handed stop mass to $M_{\tilde{t}}=200$ GeV in (a,b), and in (c,d) we use the ''LEP2 II Scan A2'' set of SUSY parameters[12] for comparison.

Because the MSSM predicts a large bottom quark Yukawa coupling for large tanβ, and the mass of the lightest neutral scalar has to be less than $\sim$130 GeV, we expect that the Tevatron and the LHC can test this model via measuring the $\phi b\bar{b}$ production rate. In the following, we shall discuss the range of the m_A-tanβ plane that can be explored at various colliders. Some models of SUSY soft-breaking predict a large tan β with light Higgs scalar(s), and thus predict a large $\phi b\bar{b}$ rate. Without observing such a signal, one can put a stringent constrain on the model. This will also be discussed below.

B. Constraints on MSSM from $\phi b\bar{b}$ production at Tevatron and LHC

To use the model-independent result of K_{min} obtained in Sec. II to constrain the m_A-tanβ plane in the MSSM, one needs to calculate the SUSY Higgs boson masses, decay

[12]The parameters m_0 and M_2 are fixed at 1 TeV, μ is chosen to be -100 GeV and $m_t=175$ GeV. The scalar trilinear coupling A_i is fixed at $\sqrt{6}$ TeV, corresponding to the maximal left- and right-handed top-squark mixing. Detailed prescription about this set of parameter scan can be found in Refs. [42,43].

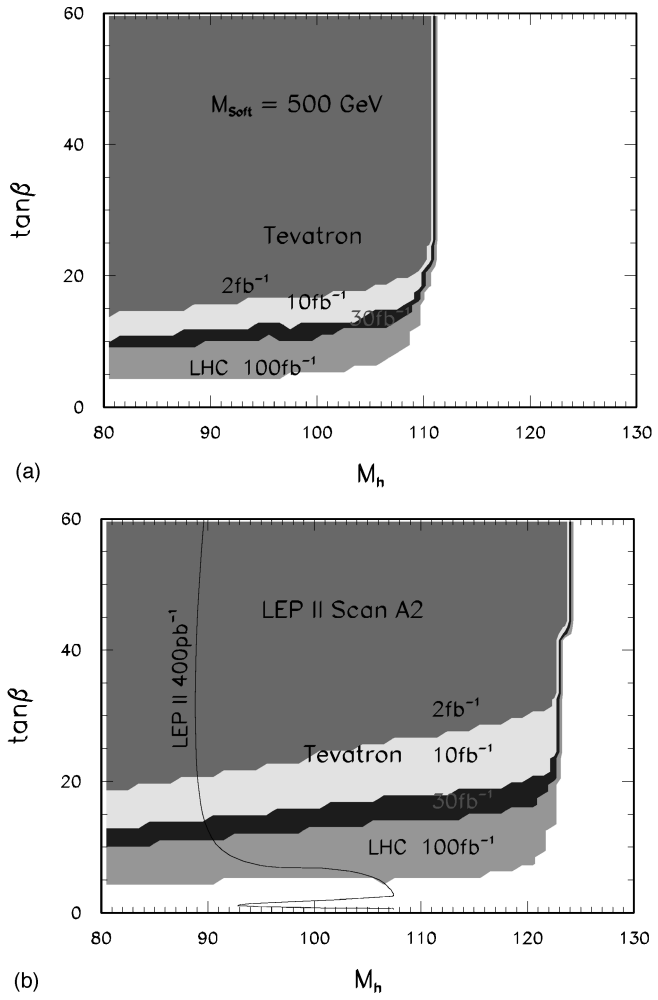

FIG. 14. 95% C.L. exclusion contours in the m_h-tanβ plane of the MSSM. The areas above the four boundaries are excluded for the Tevatron run II with the indicated luminosities, and for the LHC with an integrated luminosity of 100 fb^{-1}. LEP II can exclude the area on the left-hand side of the solid curve in the lower plot.

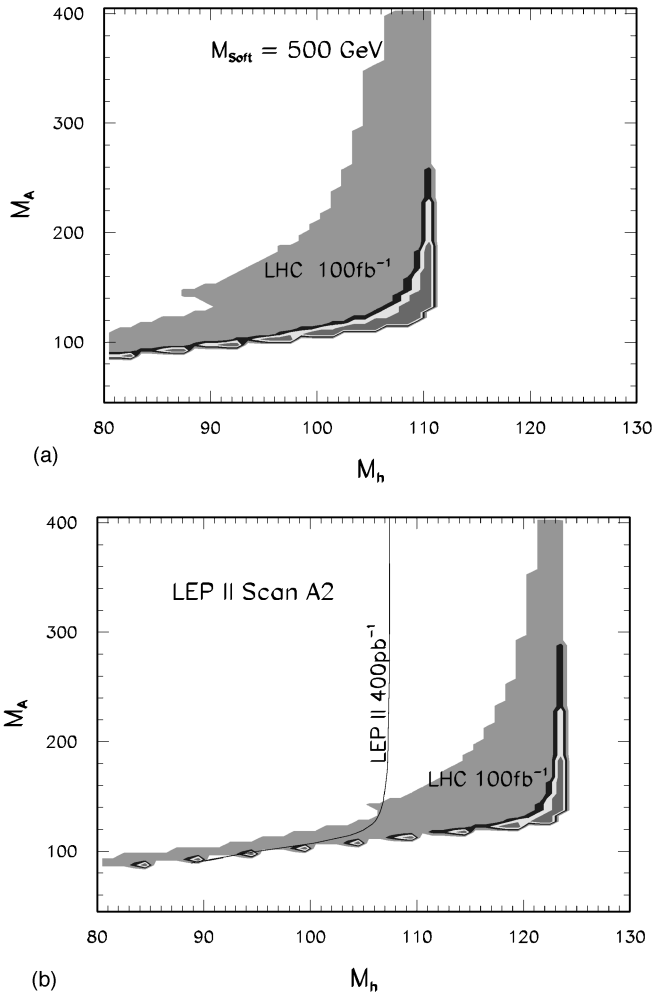

FIG. 15. 95% C.L. exclusion contours in the m_A-m_h plane of the MSSM. The shaded areas indicate the excluded regions for the Tevatron run II with integrated luminosities, 2, 10, 30 fb^{-1}, and for the LHC with an integrated luminosity of 100 fb^{-1}, as those in the previous figures. LEP II can exclude the area on the left-hand side of the solid curve in the lower plot.

branching ratios, and their couplings to the bottom quark for a given set of the soft breaking parameters. In the following numerical analysis, we use the HDECAY code to include the full mixings in the stop-sbottom sector with QCD and electroweak radiative corrections [35]. For simplicity, we assume that the superpartners are all heavy enough so that the decays of the Higgs bosons into them are forbidden. Under this assumption, we find that the decay branching ratio of $h\to b\bar{b}$ is close to one for the relevant region of the parameter space.

As explained above, we combine signals from more than one scalar boson provided their masses differ by less than $\Delta m_{\rm exp}$, which is the maximum of the experimental mass resolution (cf. footnote 7) and the natural decay width of the scalar boson. Since the results of Sec. II are given in terms of the minimal enhancement factor $K_{\rm min}$ defined in Eq. (1), we need to convert them into exclusion bounds in the m_A-tanβ plane of the MSSM, in case that a signal is not found. The bound on tan$\beta_{\rm min}$ (with the possible mass degeneracy included) can be derived from that on $K_{\rm min}$ (for a single scalar) by requiring

$$\tan^2\beta\ {\rm BR}(A\to b\bar{b})+\sum_{\phi=h,H}\theta(\Delta m_{\rm exp}-|\Delta M_{A\phi}|)\times\left(\frac{y_b^{\phi}}{y_b^{\rm SM}}\right)^2{\rm BR}(\phi\to b\bar{b})\ \geq\ K_{\rm min}^2, \tag{26}$$

where $y_b^{\rm SM}$ and y_b^{ϕ} denote the b quark Yukawa coupling in the SM and the MSSM (with $\phi=h$ or H), respectively. Inside the argument of the θ-function, $\Delta M_{A\phi}$ is the mass difference between A and ϕ. Thus, the equality sign in the above relation determines the minimal value tan$\beta_{\rm min}$ for each given $K_{\rm min}$.

To estimate the exclusion regions in the m_A-tanβ plane, a set of soft breaking parameters has to be chosen, which should be compatible with the current data from the LEP II

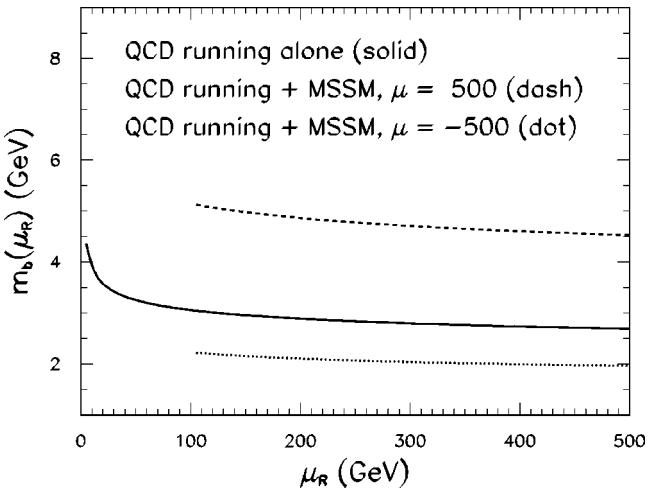

FIG. 16. The running of the bottom quark mass $m_b(\mu_R)$ as a function of the renormalization scale μ_R. The solid curve shows the QCD evolution alone. The dashed curve further includes the supersymmetric corrections to the ''effective'' running mass, for $\tan\beta=30$. All soft SUSY breaking parameters have been fixed as 500 GeV. The dotted curve includes the SUSY corrections but with the sign of the Higgs-mixing parameter μ flipped.

and the Tevatron experiments, while not much larger than 1 TeV. For simplicity, we choose all the soft SUSY breaking parameters (and the Higgs mixing parameter-μ) to be 500 GeV as our ''default'' values, i.e., $M_{\rm soft}=500\,{\rm GeV}$. In Fig. 12(a), we show the 95% C.L. exclusion contours in the m_A-tanβ plane derived from the measurement of $p\bar{p}/pp \to \phi b\bar{b} \to b\bar{b}b\bar{b}$, using this ''default'' set of SUSY parameters. The areas above the four boundaries are excluded for the Tevatron run II with the indicated luminosities, and for the LHC with an integrated luminosity of $100\,{\rm fb}^{-1}$. Needless to say, different choice of SUSY parameters, such as the mass and the mixing of the top squarks and the value (and sign) of the parameter μ, would modify this result. To compare the potential of the Tevatron and the LHC in constraining the MSSM parameters via the $\phi b\bar{b}$ ($\phi=h,A,H$) production to that of the LEP II experiments via $Z\phi$ and hA production, we consider one of the ''benchmark'' parameter scans discussed in [42,43], which is called the ''LEP II Scan A2'' [12] set. For this set of SUSY parameters, the LEP II exclusion contour [42,43] at the 95% C.L. is displayed in Fig. 12(b), for a center-of-mass energy of 200 GeV and an integrated luminosity of $100\,{\rm pb}^{-1}$ per LEP II experiment. As shown in Fig. 12(b), the Tevatron run II result, in comparison with the LEP II result, can already cover a substantial region of the parameter space with only a $2\,{\rm fb}^{-1}$ luminosity. Thus, detecting the $\phi b\bar{b}$ signal at hadron colliders can effectively probe the MSSM Higgs sector, especially for models with large tanβ values. Furthermore, for $m_A \gtrsim 100\,{\rm GeV}$, Tevatron run II is complementary with LEP II, because the latter is not sensitive to that region of parameter space. The LHC can further probe the MSSM down to $\tan\beta \sim 7(15)$ for $m_A < 400(1000)$ GeV. This is also shown in Fig. 13 using the ''default'' set of SUSY parameters, in which the region above the upper curve is the discovery contour at the 5σ level for the LHC with an integrated luminosity of $100\,{\rm fb}^{-1}$, and the area above the lower curve can be excluded at 95% C.L., if a signal is not found.

For completeness, we also present the exclusion contours in the m_h-tanβ and m_A-m_h planes for both the ''default'' and the ''LEP II Scan A2'' sets of SUSY parameters. They are shown in Figs. 14 and 15. Again, we see that the Tevatron run II and the LHC bounds sensitively and complementarily cover the MSSM parameter space in contrast to the LEP II results. We have also studied the bounds with the ''LEP II Scan A1'' inputs [42,43] and found that the exclusion contours from the $\phi b\bar{b}$ production are similar to those with ''LEP II Scan A2'' inputs. The most noticeable difference is that the theoretically allowed range for m_h becomes smaller by about 10 GeV in the ''Scan A1'' set, as compared to the ''Scan A2'' inputs.

Even though our analyses, described above and in Sec. II, are quite different from that of Ref. [8], the final bounds at the LHC happen to be in qualitative agreement. We also note that our bounds on the m_A-tanβ plane improve considerably the one obtained in Ref. [44], in which the $p\bar{p} \to \phi b\bar{b} \to \tau^+\tau^- b\bar{b}$ production rate at the Tevatron run I data was compared to the MSSM prediction. Though, we do not choose to explicitly present projected results for the Tevatron run I data, we encourage our experimental colleagues to pursue this analysis on the existing run I data sample, as it seems likely that one could obtain useful information even with the lower luminosity and collider energy of run I as well as a somewhat lower b-tagging efficiency.

Before concluding this subsection, we remark upon the effects on our bounds from the possible radiative corrections to the $\phi b\bar{b}$ production process.[13] As mentioned earlier in Sec. II, one of the dominant correction is from the next-to-leading order (NLO) QCD loops, which are not currently available for the $\phi b\bar{b}$ signal and background cross sections. However, aside from the QCD corrections to the $\phi b\bar{b}$ vertex (part of that can be simply included into the running of the $\phi b\bar{b}$ Yukawa coupling or the running b-mass), there are pentagon loops formed by the virtual gluons radiated from an initial state quark (gluon) and re-absorbed by the final state b quark with the $\phi b\bar{b}$ vertex included in the loop. Such QCD corrections are not factorizable so that a consistent improvement of our results is impossible before a full NLO QCD analysis is completed.[14] Putting aside the complexity of the full NLO QCD corrections, we briefly comment upon how the radiative corrections to the running $\phi b\bar{b}$ Yukawa coupling affect our final bounds. The well-known QCD correction, Eq. (12), alone will reduce the running mass $m_b(\mu)$ by about 40% from the scale $\mu=m_b^{\rm pole}\simeq 5$ GeV up to the weak scale of $O(200)$ GeV (cf. the solid curve of Fig. 16). This is however not the full story. The complexity comes from the

[13]This point has also been recently discussed in Ref. [45].

[14]Such a full NLO QCD calculation is beyond the scope of our current study. A systematic calculation for this is in progress [46].

finite SUSY threshold correction in the large $\tan\beta$ region which are potentially large [47–49]. In this case, as shown in Ref. [48], the dominant one-loop SUSY correction contributes to running b-mass a finite term so that $m_b(\mu)$ at the SUSY scale $\mu \equiv \mu_R = M_{\rm soft}$ is multiplied by a constant factor $1/[1+\Delta_b({\rm SUSY})]$, which appears as a common factor in the bottom Yukawa couplings of all three neutral Higgs bosons. For large $\tan\beta$, $\Delta_b({\rm SUSY})$ contains the following $\tan\beta$-enhanced terms from sbottom-gluino and stop-chargino loops:[15]

$$\Delta_b({\rm SUSY}) = \left(\frac{\Delta m_b}{m_b}\right)^{\tilde{b}\tilde{g}} + \left(\frac{\Delta m_b}{m_b}\right)^{\tilde{t}\tilde{\chi}} = \frac{-\mu \tan\beta}{16\pi^2}\left\{\frac{8}{3} g_3^2 m_{\tilde{g}} F(m_{\tilde{b}}, m_{\tilde{b}}, m_{\tilde{g}}) + [y_t A_t F(m_{\tilde{t}}, m_{\tilde{t}}, \mu) - g_2^2 M_2 F(m_{\tilde{t}}, m_2, \mu)]\right\}, \tag{27}$$

with the function F defined as

$$F(\sqrt{x}, \sqrt{y}, \sqrt{z}) = -\frac{xy \ln x/y + yz \ln y/z + zx \ln z/x}{(x-y)(y-z)(z-x)}.$$

In these equations, the MSSM Higgs parameter μ should not be confused with the usual renormalization scale μ_R. In Eq. (27), we have assumed, for simplicity, mass degeneracy for the top and bottom squarks, respectively. Equation (27) shows that the SUSY correction to the running m_b is proportional to $\tan\beta$ and μ. Thus, this correction is enhanced for large $\tan\beta$ and non-negligible in comparison with the QCD corrections. Also changing the sign of μ will vary the sign of the whole correction $\Delta_b({\rm SUSY})$ and implies that the SUSY correction can either increase or decrease the running b-mass at the energy scale around of $O(M_{\rm soft})$. Normally, when defining the running coupling using the Collins-Wilczek-Zee (CWZ) scheme [50], only the μ_R-dependent contributions are included while all the μ_R-independent terms are absorbed into the corresponding Wilson coefficient functions. However, since the μ_R-independent contribution $\Delta_b({\rm SUSY})$ is not small for large $\tan\beta$ and a full NLO SUSY calculation is not yet available, we include $\Delta_b({\rm SUSY})$ to define an ''effective'' running coupling-mass of b-quark even below the SUSY threshold scale $M_{\rm soft}$. This could give a rough estimate on the large SUSY loop corrections from the ϕ-b-$\bar{b}$ vertex. Obviously, when μ_R is much smaller than $M_{\rm soft}$, the CWZ scheme should be used. Hence, in Fig. 16, we only show the ''effective'' running mass $m_b(\mu)$ down to about 100 GeV which is the relevant energy scale and the mass scale ($\sim M_{\rm Higgs}$) considered in this paper. Figure 16 illustrates that due to the SUSY correction the ''effective'' running b mass at the weak scale can be either larger or smaller than the SM QCD running value ($\sim$3 GeV), depending on the choice of the sign of μ parameter (and also other soft-breaking parameters such as the trilinear coupling A_t and masses of the gluino, gaugino, stop and sbottom). For the ''default'' set of SUSY parameters used in our analysis, all the soft-breaking parameters are set to 500 GeV for simplicity. It happens to be the case that the SM QCD and SUSY corrections nearly cancel each other so that the ''effective'' running mass m_b is very close to the pole mass value ($\sim$5 GeV) for the scale above $\sim$100 GeV (cf. upper curve of Fig. 16). For comparison, in our analysis using the ''LEP II Scan A2'' set of SUSY parameters, the SM QCD and SUSY corrections do not cancel and tend to reduce the ''effective'' running b-mass or the Yukawa coupling $y_b(\mu)$ which results in a weaker bound for the Tevatron run II and the LHC, as shown in Fig. 12(b).[16] The difference in the exclusion contours shown in Figs. 12(a) and 12(b), derived from the measurement of the $\phi b\bar{b}$ production rate at hadron colliders, is mainly due to the difference in the ''effective'' running coupling or mass (including the QCD and SUSY corrections), as described above.[17] We therefore conclude that a full NLO QCD calculation is important for a consistent improvement of our current analysis.

C. Interpretation of results for models of soft breaking parameters

The MSSM allows for a very general set of soft SUSY-breaking terms and thus is specified by a large number of free parameters ($\simeq$124 [6]), though only a complicated subset of this parameter space is consistent with all current experimental results. It is therefore important to understand the mechanism of supersymmetry breaking (which presumably occurs at a high energy scale [51]) and to predict the soft parameters at the weak scale from an underlying model. Many alternative ideas about how supersymmetry might be broken, and how this will result in the low energy soft breaking parameters exist in the literature, including the supergravity inspired (SUGRA) models and gauge-mediated SUSY breaking (GMSB) models. In this section we examine the sensitivity of the $\phi b\bar{b}$ process to probe a few models of SUSY breaking, concentrating for the most part on the popular SUGRA and GMSB models. However, there are also other interesting ideas to which the $\phi b\bar{b}$ process may provide interesting information, because these models naturally prefer a large $\tan\beta$. A few examples include the SO(10) grand unification theories [52] [SO(10) GUTs]; the infrared fixed-point scenario [53]; and also a scenario with compositeness, the ''more minimal supersymmetric SM'' [54].

[15] We thank K. Matchev for discussing his published results in Ref. [48], and to him and W. A. Bardeen for discussing the issue of the running b-mass. Our convention of the MSSM Higgs parameter μ differs from that of Ref. [48] by a minus sign.

[16] A detailed analysis of these effects at the Tevatron run II is currently underway [45].

[17] From Fig. 12, it is also clear that, for the LHC bounds, the SUSY correction has much less impact since the relevant $\tan\beta$ values become much lower, around of $O(2-15)$.

1. Supergravity models with large tanβ

The supergravity inspired (SUGRA) models [55] incorporate gravity in a natural manner, and solve the problem of SUSY breaking through the introduction of a hidden sector, which breaks SUSY at a very high scale [$\sim O(10^{11})$ GeV] and interacts with the MSSM fields only gravitationally. This model offers an exciting glimpse into the possible connection between the heavy top quark and the EWSB by allowing radiative breaking of the electroweak symmetry, in which the large top quark Yukawa coupling can drive one of the Higgs masses negative at energy scales $\sim m_Z$. In the limit of large tanβ the bottom and tau Yukawa couplings can also play an important role [56].

Under the assumption that the gravitational interactions are flavor-blind, this model determines the entire SUSY spectrum in terms of five free parameters (at the high energy scale of the SUSY breaking) including a common scalar mass ($\tilde{m}_0$), a common gaugino mass (M), a common scalar tri-linear interaction term (A), tanβ, and the sign of the Higgs mixing parameter (sign(μ)). The weak scale particle spectrum can then be determined by using the renormalization group analysis to run the sparticle masses from the high scale to the weak scale.

Though large tanβ is not required by the minimal SUGRA model, it can naturally be accommodated, as demonstrated in [56,57], where it was found that a large tanβ also generally requires that the pseudoscalar Higgs mass be light ($m_A \leqslant 200$ GeV for tan$\beta \geqslant 30$), because the enhanced b and τ Yukawa couplings act through the renormalization group equations to reduce the down-type Higgs mass term at the weak scale, thus resulting in a light Higgs spectrum. Since the importance of the b and τ effects in the RG analysis increases with larger tanβ, as tanβ increases the resulting m_A decreases, making the large tanβ scenario in the SUGRA model particularly easy to probe through the $\phi b\bar{b}$ process. From the limits on the m_A-tanβ plane derived above in Sec. IV B, it thus seems likely that from the data of the Tevatron run II with 2 fb^{-1} of integrated luminosity, a large portion of the minimal SUGRA model with tan$\beta \geqslant 20$ may be excluded.

2. Gauge-mediated SUSY breaking models with large tan β

Models with GMSB break SUSY at a scale which is typically much lower than that present in the SUGRA models. The supersymmetry is generally broken in a hidden sector which directly couples to a set of messenger chiral superfields. This induces a difference in mass between the fermion and scalar components of the messenger fields, which in turn generates masses for the gauginos and sfermions of the MSSM fields via loops involving the ordinary gauge interactions [58,59]. A generic feature of this scenario is that because of the relatively low scale of SUSY breaking, the gravitino acquires a much smaller mass than in the SUGRA scenarios, and is generally the lightest supersymmetric partner (LSP). While specific models of GMSB vary as to their assumptions and relevant parameters, generally what must be assumed is the field content of the messenger sector (including transformation properties under the gauge group and number of multiplets in the theory) and the scale at which SUSY is broken in the hidden sector.

The minimal GMSB models can also result in a radiative breaking of the EWSB, through the renormalization group evolution of the Higgs masses (driven by the large top Yukawa coupling) from the effective SUSY breaking scale to the weak scale. As in the SUGRA model case, this evolution can drive the mass term of the up-type Higgs negative at the weak scale, thus breaking the electroweak symmetry. In fact, because the effective SUSY breaking scale in a GMSB model is typically much lower than in the SUGRA model (and thus closer to the weak scale), in order for the proper EWSB to occur, it was demonstrated in Ref. [60] that a large tanβ is required to be about 30–40. However, because the effective SUSY breaking scale is typically much lower than in the SUGRA model, the large effects of the b and τ on the Higgs mass running do not reduce the Higgs spectrum to the degree that occurs in the SUGRA model with large tanβ, and thus result in a heavier A with mass of about 400 GeV. So, this particular model would only be explored through the $\phi b\bar{b}$ process at the LHC. However, more general analyses of the GMSB scenario [61–64], introducing more degrees of freedom in the messenger sector than the minimal model, can allow for large tanβ and relax m_A to be as low as about 200 GeV. Thus, through the $\phi b\bar{b}$ production these more general models can be first probed at the Tevatron for the relevant mass range, and then largely explored at the LHC.

V. CONCLUSIONS

It remains a challenging task to determine the underlying dynamics of the electroweak symmetry breaking and the flavor symmetry breaking. Either fundamental or composite Higgs boson(s) may play a central role in the mass generation of the weak gauge bosons and the fermions. The heavy top quark, with a mass on the same order as the scale of the electroweak symmetry breaking, suggests that the top quark may play a special role in the mechanism of mass generation. In this work, we have shown that in the typical models of this type, the bottom quark, as the weak isospin partner of the top quark, can also participate in the dynamics of mass generation, and serves as an effective probe of the possible new physics associated with the Higgs boson and top quark sectors.

We have presented a model-independent analysis on Higgs boson production in association with bottom quarks, via the reaction $p\bar{p}/pp \to \phi b\bar{b} \to b\bar{b}b\bar{b}$, at the Tevatron run II and the LHC. We have computed the QCD $b\bar{b}b\bar{b}$ and $b\bar{b}jj$ backgrounds, and the electroweak $Zb\bar{b}$ background to illustrate that it is possible to extract the signal from these large backgrounds by employing a suitable search strategy. The scale and the PDF dependencies in our signal and background calculations are also examined and they indicate that the NLO QCD corrections to the production rate could be large, and thus including the complete NLO QCD corrections in future improvements will be very useful. Using the complete tree level calculation with an estimated QCD

k-factor of 2, we derive the exclusion contour for the enhancement factor (in the coupling of $\phi b\bar{b}$ relative to that of the SM) versus the Higgs mass m_ϕ at the 95% C.L., assuming a signal is not found.

We apply these results to analyze the constraints on the parameter space of both the composite models and the MSSM (in the large $\tan\beta$ region) with naturally large bottom Yukawa couplings. For the composite Higgs scenario, we first consider the two-Higgs-doublet extension of top-quark condensate model and then analyze the top-color model, where the b quark Yukawa couplings are naturally large due to the infrared quasi-fixed-point structure and the particular boundary conditions for (y_b, y_t) at the compositeness scale. Our analysis shows that the Tevatron run II with a 2 fb^{-1} of luminosity can exclude the entire parameter space of the simplest two-Higgs-doublet extension of the top-quark condensate model, if a signal is not found. For the top-color model, the Tevatron run II is able to detect the composite Higgs h_b or A_b up to ~ 400 GeV and the LHC can extend the mass range up to ~ 1 TeV. Similarly, this production mechanism can be used to effectively test the dynamical left-right symmetric model.

To confirm the MSSM, it is necessary to detect all the predicted neutral Higgs bosons (h^0, H^0, A^0) and the charged scalars ($H^\pm$). From LEP II, depending on the choice of the MSSM soft-breaking parameters, the current 95% C.L. bounds on the masses of the MSSM Higgs bosons are about 70 GeV for both the CP-even scalar h^0 and the CP-odd scalar A^0 [65]. It can be improved at LEP II with higher luminosity and maximal energy, but the bounds on the Higgs masses will not be much larger than $\sim m_Z$ for an arbitrary $\tan\beta$ value. The Wh^0 and WH^0 associated production at the Tevatron run II can further improve these bounds, if a signal is not observed. At the LHC, a large portion of parameter space can be tested via $pp \to t\bar{t} + h(\to \gamma\gamma) + X$, and $pp \to h(\to ZZ^*) + X$, etc. [66,67]. A future high energy e^+e^- collider will fully test the MSSM Higgs sector [68,69] through the reactions $e^+e^- \to Z + h(H)$, $A + h(H)$, H^+H^-, etc. In this paper, we demonstrate that studying the $\phi b\bar{b}$ channel at hadron colliders can further improve our knowledge on MSSM. The exclusion contours on the m_A-$\tan\beta$ plane of the MSSM shows that the Tevatron and the LHC are sensitive to a large portion of the parameter space via this mode. It therefore provides a complementary probe of the MSSM Higgs sector in comparison with that from LEP II. The implications of these bounds in the parameter space on both the supergravity and the gauge-mediated SUSY breaking models are further discussed. We find that the $\phi b\bar{b}$ process can effectively test the models with either scheme of the SUSY soft-breaking in the large $\tan\beta$ scenario.

In conclusion, the stringent constraints obtained by studying the associated $\phi b\bar{b}$ production at hadron colliders for both the composite and the supersymmetric models show the utility of this search mode. However, much work remains to be done. For example, a b-trigger would be essential for this analysis. The CDF group at the Fermilab has demonstrated that it is possible to detect events with four or more jets and two or more b-tags [70], which can be significantly improved with the implementation of b-trigger at the run II of the Tevatron [71]. However, the large QCD 4-jet background rate at the LHC can potentially make triggering on the $b\bar{b}\phi(\to b\bar{b})$ events difficult, though it is expected that a b-trigger would become more efficient for a heavier (pseudo-)scalar ϕ. (This is because the b-jets from the decay of a heavier ϕ are more energetic, and its QCD background rate drops rapidly as a function of the transverse momentum of the triggered jet.) We hope that the interesting results afforded by studying this channel will stimulate interest of our experimental colleagues in working on these problems.

We have found that the $\phi b\bar{b}$ process complements Higgs searches in other channels, and thus it is expected that experimental searches for this signature at the Tevatron run II (and possibly beyond) and the CERN LHC will provide interesting and important information about the mechanism of the electroweak symmetry breaking and the fermion mass generation.

ACKNOWLEDGMENTS

We thank W. A. Bardeen, E. L. Berger, B. A. Dobrescu, K. T. Matchev, C. Schmidt, M. Spira, W. K. Tung, R. Vilar and H. Weerts for useful discussions, and C. Rembser for providing us the updated LEP II data on the MSSM. We are also indebted to C. T. Hill for discussing the top-color model and M. Lindner for discussing the dynamical left-right symmetric model. We are grateful to S. Mrenna for help on checking Monte Carlo simulations and to him and M. Carena for conversations on the MSSM phenomenology. C.B. and H.J.H. thank the Theory Division of FermiLab for the invitation and hospitality. C.B., H.J.H. and C.P.Y. are supported in part by the U.S. NSF grant PHY-9507683, and J.L.D.C. and C.P.Y. by the CONACYT-NSF international agreement. T.T.'s work was done at Argonne National Lab, HEP division, and was supported in part by the U.S. DOE Contract W-31-109-Eng-38.

[1] For reviews, see e.g., G. Kane, *Perspective on Higgs Physics*, 2nd ed. (World Scientific, Singapore, 1998); T. L. Barklow *et al.*, ''New Directions for High Energy Physics,'' Snowmass, CO, 1996, hep-ph/9704217; H. Haber, in *The Higgs Puzzle: What Can We Learn From LEP2, LHC, NLC and FMC*, edited by B. A. Kniehl (World Scientific, Singapore, 1997), hep-ph/9703381; J. F. Gunion, ''Detecting and Studying Higgs Bosons,'' hep-ph/9705282; J. F. Gunion, H. E. Haber, G. Kane, and S. Dawson, *The Higgs Hunter's Guide*, 2nd ed. (Addison-Wesley, Reading, MA, 1996).

[2] CDF Collaboration, F. Abe *et al.*, Phys. Rev. Lett. **74**, 2626 (1995); **77**, 438 (1996); D0 Collaboration, S. Abachi *et al.*, *ibid.* **74**, 2632 (1995); P. Giromini, Proceedings of the Lepton-Photon Symposium, Hamburg, 1997.

[3] For a review, G. Cvetic, Rev. Mod. Phys. (to be published), hep-ph/9702381, and references therein.

[4] L. Ibanez, Nucl. Phys. **B218**, 514 (1983); J. Ellis, D. Nanopolous, and K. Tamvakis, Phys. Lett. **121B**, 123 (1983); L.

Alvare-Gaume, J. Polchinski, and M. Wise, Nucl. Phys. **B221**, 495 (1983).
[5] C. T. Hill, Phys. Rev. D **24**, 691 (1981).
[6] For examples, J. Gunion and H. Haber, Nucl. Phys. **B272**, 1 (1986); H. Haber, hep-ph/9306207; Nucl. Phys. B (Proc. Suppl.) **62**, 469 (1998); hep-ph/9703391; S. Dawson, hep-ph/9612229; S. P. Martin, hep-ph/9709356.
[7] J. L. Diaz-Cruz, H.-J. He, T. Tait, and C.-P. Yuan, Phys. Rev. Lett. **80**, 4641 (1998).
[8] J. Dai, J. Gunion, and R. Vega, Phys. Lett. B **345**, 29 (1995); **387**, 801 (1996).
[9] M. A. Luty, Phys. Rev. D **41**, 2893 (1990); M. Suzuki, *ibid.* **41**, 3457 (1990).
[10] C. T. Hill, Phys. Lett. B **345**, 483 (1995); in Proceedings of Strongly Coupled Gauge Theories, 1996, Nagoya, Japan, hep-ph/9702320.
[11] M. Lindner, hep-ph/9704362; E. Akhmedov, M. Lindner, E. Schnapka, and J. W. F. Valle, Phys. Rev. D **53**, 2752 (1996); Phys. Lett. B **368**, 270 (1996); M. Lindner and E. Schnapka, in *Heavy Flavours II*, edited by A. Buras and M. Linder (World Scientific, Singapore, 1995), hep-ph/9712489.
[12] W. A. Bardeen, C. T. Hill, and M. Lindner, Phys. Rev. D **41**, 1647 (1990).
[13] H. P. Nilles, Phys. Rep. **110**, 1 (1984); H. Haber and G. L. Kane, *ibid.* **117**, 75 (1985).
[14] For a recent review, G. F. Giudice and R. Rattazzi, Report No. CERN-TH-97, hep-ph/9801271.
[15] J. C. Collins and W.-K. Tung, Nucl. Phys. **B278**, 934 (1986); D. A. Dicus and S. Willenbrock, Phys. Rev. D **39**, 751 (1989).
[16] V. Barger, A. L. Stange, and R. J. N. Phillips, Phys. Rev. D **44**, 1987 (1991); J. F. Gunion and Z. Kunszt, Phys. Lett. **159B**, 167 (1985); Phys. Lett. B **176**, 477 (1986).
[17] W. F. Long and T. Stelzer, Comput. Phys. Commun. **81**, 357 (1994).
[18] M. Mangano, P. Nason, and G. Ridolfi, Nucl. Phys. **B373**, 295 (1992).
[19] S. Dawson and L. Reina, Phys. Rev. D **57**, 5851 (1998).
[20] CTEQ Collaboration, H. Lai, J. Huston, S. Kuhlmann, F. Olness, J. Owens, D. Soper, W.-K. Tung, and H. Weerts, Phys. Rev. D **55**, 1280 (1997).
[21] D. Amidei and R. Brock, ''Report of the *TeV*2000 Study Group on Future Electroweak Physics at the Tevatron,'' 1995.
[22] E. Richter-Was and D. Froidevaux, Z. Phys. C **76**, 665 (1997).
[23] T. Sjostrand, Comput. Phys. Commun. **82**, 74 (1994); S. Mrenna, *ibid.* **101**, 232 (1997).
[24] A. Martin, R. Roberts, M. G. Ryskin, and W. J. Stirling, Eur. Phys. J. C **2**, 287 (1998).
[25] K. Lane and E. Eichten, Phys. Lett. B **352**, 382 (1995).
[26] R. S. Chivukula and H. Georgi, Phys. Rev. D **58**, 075004 (1998); **58**, 115009 (1998).
[27] Y. Nambu, in *New Theories in Physics*, Proceedings of the XI International Symposium on Elementary Particle Physics, edited by Z. Ajduk *et al.* (World Scientific, Singapore, 1988), pp. 1–10.
[28] B. A. Dobrescu and C. T. Hill, Phys. Rev. Lett. **81**, 2634 (1998); R. S. Chivukula, B. A. Dobrescu, H. Georgi, and C. T. Hill, Phys. Rev. D (to be published), hep-ph/9809470.
[29] C. D. Froggatt, I. G. Knowles, and R. G. Moorhouse, Phys. Lett. B **298**, 356 (1993).
[30] Y. Nambu and G. Jona-Lasinio, Phys. Rev. **122**, 345 (1961).
[31] D. Bjorken, Ann. Phys. (N.Y.) **24**, 174 (1963); T. Equchi, Phys. Rev. D **14**, 2755 (1976).
[32] C. T. Hill, C. Leung, and S. Rao, Nucl. Phys. **B262**, 517 (1985).
[33] For example, V. Barger, M. S. Berger, and P. Ohmann, Phys. Rev. D **47**, 1093 (1993), and references therein.
[34] Particle Data Group, R. M. Barnett *et al.*, Phys. Rev. D **54**, 1 (1996).
[35] A. Djouadi, J. Kalinowski, and M. Spira, Comput. Phys. Commun. **108**, 56 (1998).
[36] H. Pagels and S. Stokar, Phys. Rev. D **20**, 2947 (1979).
[37] S. Weinberg, Phys. Rev. D **19**, 1277 (1979); L. Susskind, *ibid.* **20**, 2619 (1979); S. Dimopoulos and L. Susskind, Nucl. Phys. **B155**, 237 (1979); E. Eichten and K. Lane, Phys. Lett. **90B**, 125 (1980).
[38] B. Holdom, Phys. Rev. D **24**, 1441 (1981); Phys. Lett. **150B**, 301 (1985); T. Appelquist, D. Karabali, and L. C. R. Wijewardhana, Phys. Rev. Lett. **57**, 957 (1986); K. Yamawaki, M. Bando, and K. Matumoto, *ibid.* **56**, 1335 (1986).
[39] D. Kominis, Phys. Lett. B **345**, 483 (1995); G. Buchalla, G. Burdman, C. T. Hill, and D. Kominis, Phys. Rev. D **53**, 5185 (1996); J. D. Wells, *ibid.* **56**, 1504 (1997).
[40] M. Lindner (private communication).
[41] Y. Okada *et al.*, Prog. Theor. Phys. Suppl. **85**, 1 (1991); H. Haber and R. Hempfling, Phys. Rev. Lett. **66**, 1815 (1991); J. Ellis *et al.*, Phys. Lett. B **257**, 83 (1991).
[42] C. Rembser, plenary talk at International Symposium on ''Frontiers of Phenomenology from Non-perturbative QCD to New Physics,'' 1998, Madison, Wisconsin.
[43] N. Konstantinidis, plenary talk at the Workshop on ''Physics at Run II–Supersymmetry/Higgs,'' First General Meeting, 1998, Fermi National Accelerator Laboratory, Batavia, Illinois.
[44] M. Drees, M. Guchait, and P. Roy, Phys. Rev. Lett. **80**, 2047 (1998); **81**, 2394(E) (1998).
[45] S. Mrenna, talk given at the Higgs Working Group meeting of the Run II Workshop, Fermilab, 1998; M. Carena, S. Mrenna, and C. E. W. Wagner (unpublished).
[46] M. Spira (private communication).
[47] R. Hempfling, Phys. Rev. D **49**, 6168 (1994); L. J. Hall, R. Rattazzi, and U. Sarid, *ibid.* **50**, 7048 (1994); M. Carena, M. Olechowski, S. Pokorski, and C. E. M. Wagner, Nucl. Phys. **B426**, 269 (1994).
[48] J. Bagger, K. Matchev, and D. Pierce, in Proceedings of Beyond the Standard Model IV, Lake Tahoe, CA, 1994, p. 363, hep-ph/9503422; D. M. Pierce, J. A. Bagger, K. Matchev, and R. J. Zhang, Nucl. Phys. **B491**, 3 (1997), and references therein.
[49] J. A. Coarasa, R. A. Jimenez, and J. Sola, Phys. Lett. B **389**, 312 (1996); R. A. Jimenez and J. Sola, *ibid.* **389**, 52 (1996).
[50] J. Collins, F. Wilczek, and A. Zee, Phys. Rev. D **18**, 242 (1978).
[51] G. L. Kane, hep-ph/9705382; Nucl. Phys. B (Proc. Suppl.) **62**, 144 (1998); J. L. Feng *et al.*, Phys. Rev. D **52**, 1418 (1995).
[52] See, for instance, L. J. Hall, R. Rattazzi, and U. Sarid, Phys. Rev. D **50**, 7048 (1994); S. Dimopoulos, L. J. Hall, and S. Raby, Phys. Rev. Lett. **68**, 1984 (1992); G. Lazarides and C. Panagiotakopoulos, Phys. Lett. B **337**, 86 (1997).
[53] See, for instance, C. D. Froggatt, R. G. Moorhouse, and I. G.

Knowles, Phys. Lett. B **298**, 356 (1993); B. Schrempp and M. Wimmer, Prog. Part. Nucl. Phys. **37**, 1 (1996), and references therein.

[54] A. Cohen, D. Kaplan, and A. Nelson, Phys. Lett. B **388**, 588 (1996).

[55] For a review, R. Arnowitt and P. Nath, hep-ph/9708254.

[56] M. Drees and M. Nojiri, Nucl. Phys. **B369**, 54 (1992).

[57] H. Baer *et al.*, Phys. Rev. Lett. **79**, 986 (1997).

[58] M. Dine, A. Nelson, Y. Nir, and Y. Shirman, Phys. Rev. D **53**, 2658 (1996).

[59] For a review, C. Kolda, Nucl. Phys. B (Proc. Suppl.) **62**, 266 (1998).

[60] K. Babu, C. Kolda, and F. Wilczek, Phys. Rev. Lett. **77**, 3070 (1996); S. Dimopoulos, M. Dine, S. Raby, and S. Thomas, *ibid.* **76**, 3494 (1996).

[61] J. A. Bagger, K. Matchev, D. M. Pierce, and R. J. Zhang, Phys. Rev. D **55**, 3188 (1997).

[62] H. Baer, M. Brhlik, C. Chen, and X. Tata, Phys. Rev. D **55**, 4463 (1997).

[63] R. Rattazzi and U. Sarid, Nucl. Phys. **B501**, 297 (1997); E. Gabrielli and U. Sarid, Phys. Rev. Lett. **79**, 4752 (1997).

[64] F. Borzumatti, hep-ph/9702307.

[65] ALEPH Collaboration, R. Barate *et al.*, Phys. Lett. B **412**, 173 (1997); DELPHI Collaboration, P. Abreu *et al.*, Eur. Phys. J. C **2**, 1 (1998); L3 Collaboration, M. Acciarri *et al.*, Phys. Lett. B **436**, 389 (1998); OPAL Collaboration, K. Ackerstaff *et al.*, Eur. Phys. J. C **5**, 19 (1998); J. F. Gunion *et al.*, 1996 DPF/DPS summer study, hep-ph/9703330.

[66] Z. Kunszt and F. Zwirner, Nucl. Phys. **B385**, 3 (1992).

[67] J. L. Diaz-Cruz and O. Sampayo, Int. J. Mod. Phys. A **8**, 4339 (1993); J. Gunion and L. Orr, Phys. Rev. D **46**, 2052 (1994); H. Baer, B. W. Harris, and X. Tata, *ibid.* **58**, 015003 (1998).

[68] See, for instance, J. F. Gunion *et al.*, 1996 DPF/DPS summer study, hep-ph/9703330; J. F Gunion, hep-ph/9801417.

[69] H. Murayama and M. E. Peskin, Annu. Rev. Nucl. Part. Sci. **46**, 533 (1997); E. Accomando *et al.*, Phys. Rep. **299**, 1 (1998).

[70] CDF Collaboration, F. Abe *et al.*, Phys. Rev. Lett. **81**, 5748 (1998).

[71] The CDF II Collaboration, ''The CDF II Detector Technical Design Report,'' Fermilab-Pub-96/390-E.